Symplectic Hamiltonian HDG methods for wave propagation phenomena

M.A. Sánchez [a,b,*], C. Ciuca [c], N.C. Nguyen [d,1], J. Peraire [d,1], B. Cockburn [a]

[a] School of Mathematics, University of Minnesota, Minneapolis, MN 55455, USA
[b] Institute for Mathematical and Computational Engineering, School of Engineering and Faculty of Mathematics, Pontificia Universidad Católica de Chile, Santiago, Chile
[c] Department of Aeronautics, Imperial College London, London SW7 2AZ, UK
[d] Department of Aeronautics and Astronautics, Massachusetts Institute of Technology, Cambridge, MA 02139, USA

ARTICLE INFO

ABSTRACT

We devise the first symplectic Hamiltonian hybridizable discontinuous Galerkin (HDG) methods for the acoustic wave equation. We discretize in space by using a Hamiltonian HDG scheme, that is, an HDG method which preserves the Hamiltonian structure of the wave equation, and in time by using symplectic, diagonally implicit and explicit partitioned Runge–Kutta methods. The fundamental feature of the resulting scheme is that the conservation of a discrete energy, which is nothing but a discrete version of the original Hamiltonian, is guaranteed. We present numerical experiments which indicate that the method achieves optimal approximations of order $k + 1$ in the L^2-norm when polynomials of degree $k \geq 0$ and Runge–Kutta time-marching methods of order $k + 1$ are used. In addition, by means of post-processing techniques and by increasing the order of the Runge–Kutta method to $k+2$, we obtain superconvergent approximations of order $k+2$ in the L^2-norm for the displacement and the velocity. We also present numerical examples that corroborate that the methods conserve energy and that they compare favorably with dissipative HDG schemes, of similar accuracy properties, for long-time simulations.

© 2017 Elsevier Inc. All rights reserved.

1. Introduction

In this paper, we devise symplectic Hamiltonian hybridizable discontinuous Galerkin (HDG) methods for numerically solving the wave equation

$$\ddot{u}(t) = \operatorname{div}(\kappa \nabla u(t)) + f(t) \qquad \text{in } \Omega, \quad \forall t \geq 0, \tag{1a}$$

$$\alpha \kappa \nabla u(t) \cdot \boldsymbol{n} + \beta u(t) = g(t) \qquad \text{on } \Gamma := \partial\Omega, \quad \forall t \geq 0, \tag{1b}$$

$$u(0) = u_0, \qquad \text{in } \Omega, \quad t = 0, \tag{1c}$$

$$\dot{u}(0) = v_0 \qquad \text{in } \Omega, \quad t = 0, \tag{1d}$$

* Corresponding author.
E-mail addresses: sanchez@umn.edu (M.A. Sánchez), cristian.ciuca13@imperial.ac.uk (C. Ciuca), cuongng@mit.edu (N.C. Nguyen), peraire@mit.edu (J. Peraire), cockburn@math.umn.edu (B. Cockburn).

on an open and bounded polygonal domain $\Omega \subset \mathbb{R}^d$ with Lipschitz continuous boundary $\Gamma := \partial\Omega$. We assume that the scalar coefficient $\kappa = \kappa(x) \in L^\infty(\Omega)$, satisfies $\kappa \geq \kappa_0 > 0$ almost everywhere, and the source term $f(t) \in L^2(\Omega)$ for all $t \geq 0$. The problem prescribes Robin boundary conditions with coefficients α, β varying on $\partial\Omega$, and the source term $g(t) \in H^{1/2}(\partial\Omega)$, for all $t \geq 0$. Initial conditions are also given, with initial data $u_0, v_0 \in L^2(\Omega)$. We are particularly interested in the case in which the wave equation system (1) is autonomous, that is, when the source terms are $f \equiv 0$ and $g \equiv 0$. Under these conditions, the energy is conserved in time which fuels the interest in the development of non-dissipative methods numerical methods, that is, of methods which also conserve a discrete version of the energy. Since most, if not all, HDG methods proposed so far are actually dissipative, it was believed that non-dissipative HDG methods did not exist. However, here we show how to devise a large class of non-dissipative HDG methods for the wave equation and argue that methods with similar conservation properties can be obtained by using mixed and standard DG methods as well.

The semi-discrete numerical scheme presented in this paper belongs to the class of HDG methods. These methods were first introduced in [12] for diffusion problems, and since then they have gained notorious attention, accumulating extensive theoretical and experimental results for a wide variety of partial differential equations. Their popularity is explained mainly by two properties, the significantly smaller number of globally-coupled unknowns compared to DG methods, and the enhanced convergence or superconvergence property of their approximations; see the recent reviews in [8,7].

The HDG methodology has also been applied to wave propagation problems. First, in [26] a semi-discrete HDG method coupled with diagonally implicit Runge–Kutta time-marching method was applied to the acoustic wave propagation and elastodynamics. The fully discrete method was implicit and high-order accurate with optimal rates of convergence, as their numerical experiments showed. The semi-discrete scheme, based on the velocity and stress variables, was later analyzed in [13], where the authors proved optimal L^2-error estimates for the velocity and stress approximations. They also proved superconvergence properties and showed a local post-processing technique that gives a superconvergent approximation to the displacement of order $k + 2$. More recently, an explicit method, based on the same semi-discrete formulation, was introduced in [31] which displayed similar convergence properties. Unfortunately, these methods are dissipative and are not suitable for long-term simulations.

Many finite element methods have been applied to wave propagation problems. In particular, mixed and discontinuous Galerkin (DG) methods have shown certain advantages in comparison with continuous finite element methods. Since the introduction of the mixed method for the velocity-stress formulation in [19], many others have considered this first order system for their discretization. For instance, space–time DG methods [18,25,27], staggered DG methods [4,5], local discontinuous Galerkin methods [32], and symmetric interior penalty methods [20]. In particular, in [20] the authors proved optimal rates of convergence in the L^2-norm. An alternative formulation for the displacement and the stress has also been discretized using mixed methods in [16]. They obtained optimal L^2-errors estimates of the semi-discrete scheme. For a complete description and comparison of these methods see [13].

In spite of the optimal convergence properties (or quasi-optimal in some cases), most of the schemes mentioned above might not be suitable for long-time computations, due to their energy-dissipative characteristics. Indeed, it has been observed that dissipative numerical schemes suffer a loss of accuracy for long-time computations, despite their optimal error estimates. The exceptions in the schemes mentioned above are the energy-conserving schemes introduced in [4,5], [23] and [32]. The proof of the energy-conservative properties in these cases uses features of the respective methods. Alternatively, there are numerical methods that derive the energy conservation from the structure of the discretization. They devise a spatial discretization satisfying a discrete Hamiltonian structure, and prove the conservation of energy by simply applying the theory of finite dimensional Hamiltonian systems. Among these methods we found, the non-dissipative DGTD method in [28], and the mimetic finite difference methods in [17]. More recently, in [14], a semidiscrete, energy-conservative HDG was proposed. Since the method keeps the second-order time derivative, it was combined with a Stormer–Numerov time-marching method. The resulting method preserves an approximation to the energy under a suitable CFL condition. In this paper, we keep the same semidiscrete HDG discretization, but introduce the velocity as a new unknown. This allows us to show that the Hamiltonian structure of the wave equation is preserved under discretization and that, as a consequence, when symplectic time-marching schemes are used, the discrete Hamiltonian of the semidiscrete scheme, the discrete energy in our case, is maintained constant in time.

Thus, the numerical methods presented in this paper have two fundamental properties. First, the L^2-errors of the approximations for the displacement, velocity, and stress (or negative gradient) variables converge optimally, with an order of $k + 1$ when piecewise polynomials of degree k are used, and a superconvergence order of $k + 2$ is achieved for the L^2 errors of the post-processed approximations for the displacement and velocity variables. Second, the discrete Hamiltonian of the space discretization, which is nothing but the discrete energy of the space discretization, remains constant in time. We focus on symplectic implicit and explicit Runge–Kutta methods of orders consistent with the superconvergence rate $k + 2$. To the best of our knowledge, these are the first symplectic Hamiltonian HDG schemes.

The paper is structured as follows. In Section 2, we introduce the Hamiltonian formulation of the wave equation and describe its HDG discretization. We then present the main result of the paper, the preservation of the Hamiltonian structure of the wave equation under the HDG discretization. In Section 3, we present the high-order accurate symplectic time-integrators that complete our fully discrete schemes. First, we introduce symplectic diagonally implicit Runge–Kutta methods, and then symplectic explicit partitioned Runge–Kutta methods. In both cases, we outline the resulting pseudo-algorithms. We then define the post-processing techniques employed to obtain superconvergent approximations in Sec-

tion 2.4. In Section 4, we present numerical evidence corroborating the expected convergence properties of the schemes and displaying their conservative properties. Finally, in Section 5, we discuss the extension of our ideas to mixed and DG methods, and briefly discuss future work.

2. The Hamiltonian HDG scheme

In this section, we introduce the semi-discrete Hamiltonian HDG method approximating solutions of the wave equation under consideration; we follow [14]. We then prove that this numerical scheme preserves the Hamiltonian structure of the continuous problem. Because of this property, which turns out to be the cornerstone in the construction of fully discrete energy-conservative schemes, the method is said to be a Hamiltonian method.

We begin by rewriting the second order partial differential equation (1a) into a Hamiltonian system for the displacement $u(t)$ and the velocity $v(t)$ variables

$$\dot{u}(t) = v(t) \qquad\qquad \text{in } \Omega, \quad \forall t \geq 0, \tag{2a}$$

$$\dot{v}(t) = f(t) - \nabla \cdot \boldsymbol{q}(t) \qquad \text{in } \Omega, \quad \forall t \geq 0, \tag{2b}$$

$$\boldsymbol{q}(t) := -\kappa \nabla u(t) \qquad\quad \text{in } \Omega, \quad \forall t \geq 0. \tag{2c}$$

These are subject to Robin boundary conditions,

$$\alpha \boldsymbol{q}(t) \cdot \boldsymbol{n} + \beta u(t) = g(t) \qquad \text{on } \Gamma, \quad \forall t \geq 0, \tag{3}$$

and the initial conditions,

$$u(0) = u_0, \quad v(0) = v_0 \qquad \text{in } \Omega, \quad t = 0. \tag{4}$$

The total Hamiltonian function associated with (2) is given by

$$H(u, v, t) = \int_{\Omega} \left(\frac{1}{2} v(t)^2 + \frac{1}{2} \kappa^{-1} \boldsymbol{q}(t) \cdot \boldsymbol{q}(t) - f(t) u(t) \right) dx - \int_{\partial \Omega} \alpha^{-1} g(t) u(t) \, ds. \tag{5}$$

If $f(t) = g(t) = 0$ then it can be easily shown that the Hamiltonian function satisfies

$$H(u(t), v(t)) = H(u(0), v(0)) = H(u_0, v_0) \geq 0, \quad \forall t. \tag{6}$$

The quantity $E(t) \equiv H(u(t), v(t))$ is called the energy of the Hamiltonian system (2), which is conserved for all time.

Next, we define the Hamiltonian HDG method based on the Hamiltonian system (2). We first introduce some standard discontinuous Galerkin notation.

2.1. Notation

Let Ω_h be a conforming simplicial triangulation of $\overline{\Omega} \subset \mathbb{R}^d$, i.e., the elements of Ω_h are segments for $d = 1$, triangles for $d = 2$, and tetrahedra for $d = 3$. We denote by $\mathcal{E}_h$ the set of faces ($d = 3$, respectively edges $d = 2$ or nodes $d = 1$) of the triangulation (or skeleton of the triangulation). We assume that the triangulation Ω_h satisfies standard finite element assumptions, see [6] and [3].

For a domain $K \in \mathbb{R}^d$ we let $(\cdot, \cdot)_K$ to be the volume integral of the inner product for functions $u, v \in L^2(K)$ and $\boldsymbol{q}, \boldsymbol{r} \in [L^2(K)]^d$, i.e.,

$$(u, v)_K := \int_K uv \, dx, \qquad (\boldsymbol{q}, \boldsymbol{r})_K := \int_K \boldsymbol{q} \cdot \boldsymbol{r} \, dx. \tag{7}$$

Similarly, for a domain $F \subset \mathbb{R}^{d-1}$ the product is denoted by $\langle \cdot, \cdot \rangle_F$, i.e., for $\mu, \eta \in L^2(F)$ we have

$$\langle \mu, \eta \rangle_F := \int_F \mu \eta \, ds. \tag{8}$$

Now, by means of the previous definitions, we introduce the following products over the triangulation and its skeleton

$$(u, v)_{\Omega_h} := \sum_{K \in \Omega_h} (u, v)_K, \qquad (\boldsymbol{q}, \boldsymbol{r})_{\Omega_h} := \sum_{K \in \Omega_h} (\boldsymbol{q}, \boldsymbol{r})_K,$$

$$\langle \cdot, \cdot \rangle_{\partial K} := \sum_{F \in \partial K \cap \mathcal{E}_h} \langle \cdot, \cdot \rangle_F, \quad \langle u, \boldsymbol{r} \cdot \boldsymbol{n} \rangle_{\partial \Omega_h} := \sum_{K \in \Omega_h} \langle u, \boldsymbol{r} \cdot \boldsymbol{n} \rangle_{\partial K},$$

$$\langle u, v \rangle_{\partial \Omega_h} := \sum_{K \in \Omega_h} \langle u, v \rangle_{\partial K}, \quad \langle u, v \rangle_{\partial \Omega_h \backslash \Gamma} := \sum_{K \in \Omega_h} \langle u, v \rangle_{\partial K \backslash (\partial K \cap \Gamma)}.$$

Furthermore, our numerical methods seek finite element approximations to the displacement u, the velocity v, and the flux $\boldsymbol{q}$ in the domain, and the displacement u on the faces of the triangulation. These numerical approximations be defined on the following discontinuous piecewise polynomial spaces:

$$\boldsymbol{V}_h := \{\boldsymbol{r} \in [L^2(\Omega)]^d : \boldsymbol{r}|_K \in \boldsymbol{V}(K), \forall K \in \Omega_h\},$$

$$W_h := \{w \in L^2(\Omega) : w|_K \in W(K), \forall K \in \Omega_h\},$$

$$M_h := \{\mu \in L^2(\mathcal{E}_h) : \mu|_F \in M(F), \forall F \in \mathcal{E}_h\}.$$

For the sake of simplicity, we take the local spaces as $\boldsymbol{V}(K) := [\mathcal{P}_k(K)]^d$, $W(K) := \mathcal{P}_k(K)$, and $M(F) := \mathcal{P}_k(F)$, where $\mathcal{P}_k(D)$ denotes the space of polynomials of degree at most k on a domain D. In this case, the definition of the HDG projection is as follows. Given $\boldsymbol{q} \in [L^2(\Omega)]^d$ and $u \in L^2(\Omega)$, the HDG projection $(\boldsymbol{\Pi}\boldsymbol{q}, \Pi u)$ is defined locally for each simplex $K \in \Omega_h$, by the solution of the following system of equations:

$$
\begin{aligned}
(\boldsymbol{\Pi}\boldsymbol{q}, \boldsymbol{r})_K &= (\boldsymbol{q}, \boldsymbol{r})_K & &\forall \boldsymbol{r} \in \mathcal{P}_{k-1}(K), \\
(\Pi u, w)_K &= (u, w)_K & &\forall w \in \mathcal{P}_{k-1}(K), \\
\langle \boldsymbol{\Pi}\boldsymbol{q} \cdot \boldsymbol{n} + \tau \Pi u, \mu \rangle_{\partial K} &= \langle \boldsymbol{q} \cdot \boldsymbol{n} + \tau u, \mu \rangle_{\partial K} & &\forall \mu \in \cup_{F \in \partial K} \mathcal{P}_k(F),
\end{aligned}
\tag{9}
$$

for τ a stabilization parameter.

The above choice of elements and local spaces is convenient for its simplicity but is certainly not necessary. Other choices of elements and local spaces can be obtained by using the theory of M-decompositions, see [11,9,10].

Now, we are in position to introduce the Hamiltonian HDG scheme.

2.2. The semi-discrete HDG formulation

We discretize the Hamiltonian form (2) of the acoustic wave equation using HDG methods. Note that, this HDG formulation is slightly different from the one introduced in [14], where the velocity variable is not approximated directly. However, the convergence results derived in [14] can be applied to this case. We define the semi-discrete HDG method as follows: find $(u_h(t), v_h(t), \boldsymbol{q}_h(t), \widehat{u}_h(t)) \in W_h \times W_h \times \boldsymbol{V}_h \times M_h$, such that

$$(\dot{u}_h(t), w)_{\Omega_h} = (v(t), w)_{\Omega_h} \tag{10a}$$

$$(\dot{v}_h(t), w)_{\Omega_h} = (\boldsymbol{q}_h(t), \nabla w)_{\Omega_h} - \langle \widehat{\boldsymbol{q}}_h(t) \cdot \boldsymbol{n}, w \rangle_{\partial\Omega_h} + (f(t), w)_{\Omega_h} \tag{10b}$$

$$(\kappa^{-1}\boldsymbol{q}_h(t), \boldsymbol{r})_{\Omega_h} = (u_h(t), \nabla \cdot \boldsymbol{r})_{\Omega_h} - \langle \widehat{u}_h(t), \boldsymbol{r} \cdot \boldsymbol{n} \rangle_{\partial\Omega_h} \tag{10c}$$

$$\langle \widehat{\boldsymbol{q}}_h(t) \cdot \boldsymbol{n}, \mu \rangle_{\partial\Omega_h \setminus \Gamma} = \langle \alpha \widehat{\boldsymbol{q}}_h(t) \cdot \boldsymbol{n} - \beta \widehat{u}_h(t) + g(t), \mu \rangle_{\Gamma} \tag{10d}$$

$$\widehat{\boldsymbol{q}}_h(t) \cdot \boldsymbol{n} := \boldsymbol{q}_h(t) \cdot \boldsymbol{n} + \tau(u_h(t) - \widehat{u}_h(t)) \qquad \text{on } \mathcal{E}_h, \tag{10e}$$

for all $w \in W_h$, $\boldsymbol{v} \in \boldsymbol{V}_h$ and $\mu \in M_h$, and for all $t \geq 0$. Moreover, the initial conditions of the system $(u_h(0), v_h(0), \boldsymbol{q}_h(0), \widehat{u}_h(0))$ are prescribed by suitable projections to the finite element spaces of the initial data (u_0, v_0). Specifically, $(u_h(0), \boldsymbol{q}_h(0), \widehat{u}_h(0)) \in W_h \times \boldsymbol{V}_h \times M_h$ are defined as the solution of the system:

$$(\kappa^{-1}\boldsymbol{q}_h(0), \boldsymbol{r})_{\Omega_h} - (u_h(0), \nabla \cdot \boldsymbol{r})_{\Omega_h} + \langle \widehat{u}_h(0), \boldsymbol{r} \cdot \boldsymbol{n} \rangle_{\partial\Omega_h} = 0 \qquad \forall \boldsymbol{r} \in \boldsymbol{V}_h \tag{11a}$$

$$-(\boldsymbol{q}_h(0), \nabla w)_{\Omega_h} + \langle \widehat{\boldsymbol{q}}_h(0) \cdot \boldsymbol{n}, w \rangle_{\partial\Omega_h} = (-\nabla \cdot (\kappa \nabla u_0), w)_{\Omega_h} \quad \forall w \in W_h, \tag{11b}$$

$$\langle \widehat{\boldsymbol{q}}_h(0) \cdot \boldsymbol{n}, \mu \rangle_{\partial\Omega_h \setminus \Gamma} + \langle -\alpha \widehat{\boldsymbol{q}}_h(0) \cdot \boldsymbol{n} + \beta \widehat{u}_h(0), \mu \rangle_{\Gamma} = \langle g(0), \mu \rangle_{\Gamma} \qquad \forall \mu \in M_h, \tag{11c}$$

$$\widehat{\boldsymbol{q}}_h(0) \cdot \boldsymbol{n} = \boldsymbol{q}_h(0) \cdot \boldsymbol{n} + \tau(u_h(0) - \widehat{u}_h(0)) \qquad \text{on } \mathcal{E}_h, \tag{11d}$$

and $v_h(0) \in W_h$ is given by

$$((\dot{\boldsymbol{q}})_h(0), v_h(0)) := (\boldsymbol{\Pi}(-\kappa \nabla v_0), \Pi(v_0)), \tag{12}$$

where $(\boldsymbol{\Pi}\boldsymbol{q}, \Pi u) \in \boldsymbol{V}_h \times W_h$ is the auxiliary HDG-projection defined in (9).

Remark 2.1. The particular choice of the initial condition (11) of the HDG method is guided by the analysis in [14]. An interesting question is if we can replace this initial condition by other projections. For instance, by the L^2-projection or by the HDG projections of the initial data. We explore these options in Section 4, finding evidence of loss of accuracy for the L^2 projection.

2.3. The Hamiltonian structure of the HDG formulation

Next, we prove that the Hamiltonian structure of the wave equation is preserved after the discretization with the HDG method. To state the result, we need introduce some notation. For the sake of simplicity, and without loss of generality, we consider an orthonormal basis $\{\phi_i\}_{i \in \mathcal{J}}$ of the finite element space W_h, that is, $(\phi_i, \phi_j)_{\Omega_h} = \delta_{i,j}$, where $\delta_{i,j}$ is the Kronecker delta function. Then, we define the degrees of freedom of the approximations $u_h(t)$ and $v_h(t)$, respectively $u_i(t)$ and $v_i(t)$, for $i \in \mathcal{J}$, by

$$u_h(t,x) = \sum_{i \in \mathcal{J}} u_i(t)\phi_i(x), \qquad v_h(t,x) = \sum_{i \in \mathcal{J}} v_i(t)\phi_i(x).$$

We can now state our main result.

Theorem 1. *Set* $\mathsf{p}_i := v_i$ *and* $\mathsf{q}_i := u_i$, *for* $i \in \mathcal{J}$, *and* $\mathcal{H}(\mathsf{p},\mathsf{q},t) := H_h(u_h, v_h, t)$ *where*

$$H_h(u_h, v_h, t) = \frac{1}{2}(v_h, v_h)_{\Omega_h} + \frac{1}{2}(\kappa^{-1}\boldsymbol{q}_h, \boldsymbol{q}_h)_{\Omega_h} + \frac{1}{2}\langle \tau(u_h - \widehat{u}_h), u_h - \widehat{u}_h \rangle_{\partial\Omega_h} - (f(t), u_h)_{\Omega_h} - \langle (\frac{1}{\alpha})g(t), \widehat{u}_h \rangle_{\partial\Omega_h}. \quad (13)$$

Here $\boldsymbol{q}_h$ *and* $\widehat{u}_h(t)$ *are determined by the HDG scheme in terms of* u_h, *by means of equations* (10c), (10d) *and* (10e). *Then, the HDG method* (10) *is equivalent to the following Hamiltonian system:*

$$\dot{\mathsf{p}}_i = -\frac{\partial}{\partial\mathsf{q}_i}\mathcal{H}(\mathsf{p},\mathsf{q},t) \quad i \in \mathcal{J},$$

$$\dot{\mathsf{q}}_i = \frac{\partial}{\partial\mathsf{p}_i}\mathcal{H}(\mathsf{p},\mathsf{q},t) \quad i \in \mathcal{J}.$$

This result states that the semi-discrete HDG method (10) has a Hamiltonian structure. A consequence of this fact is that the discrete Hamiltonian, which in this case is also a discrete energy, remains constant in time whenever $H_h(u_h, v_h, t) = H_h(u_h, v_h)$, that is, whenever f and g are independent of time. Indeed, in such a case we have that

$$\frac{d}{dt}H_h(u_h, v_h) = \dot{\mathcal{H}}(\mathsf{p},\mathsf{q}) = \dot{\mathsf{p}}_i\frac{\partial\mathcal{H}}{\partial\mathsf{p}_i} + \dot{\mathsf{q}}_i\frac{\partial\mathcal{H}}{\partial\mathsf{q}_i} = -\frac{\partial\mathcal{H}}{\partial\mathsf{q}_i}\frac{\partial\mathcal{H}}{\partial\mathsf{p}_i} + \frac{\partial\mathcal{H}}{\partial\mathsf{p}_i}\frac{\partial\mathcal{H}}{\partial\mathsf{q}_i} = 0.$$

Another consequence is that this spatial discretization is a proper pair for symplectic time integrators, see [30,21], as the resulting fully discrete method always maintain a modified Hamiltonian constant in (discrete) time. Moreover, since our Hamiltonian is quadratic, exact Hamiltonian conservation is achieved by means of Runge–Kutta methods that preserve quadratic invariants. These methods are symplectic [2].

Let us prove Theorem 1.

Proof. Let us prove the first identity. We have

$$\begin{aligned}
\dot{\mathsf{p}}_i &= \dot{v}_i && \text{by def. of } \mathsf{p}_i,\\
&= (\dot{v}_h, \phi_i)_{\Omega_h} && \text{by def. of } \phi_i,\\
&= (\nabla\phi_i, \boldsymbol{q}_h)_{\Omega_h} - \langle \phi_i, \widehat{\boldsymbol{q}}_h \cdot \boldsymbol{n} \rangle_{\partial\Omega_h} + (\phi_i, f(t))_{\Omega_h} && \text{by (10b)},\\
&= -(\phi_i, \nabla\cdot\boldsymbol{q}_h)_{\Omega_h} - \langle \phi_i, (\widehat{\boldsymbol{q}}_h - \boldsymbol{q}_h)\cdot\boldsymbol{n} \rangle_{\partial\Omega_h} + (\phi_i, f(t))_{\Omega_h}\\
&= -(\frac{\partial}{\partial u_i}u_h, \nabla\cdot\boldsymbol{q}_h)_{\Omega_h} - \langle \frac{\partial}{\partial u_i}u_h, (\widehat{\boldsymbol{q}}_h - \boldsymbol{q}_h)\cdot\boldsymbol{n} \rangle_{\partial\Omega_h} + (\frac{\partial}{\partial u_i}u_h, f(t))_{\Omega_h} && \text{by def. of } \phi_i,\\
&= -(\frac{\partial}{\partial u_i}u_h, \nabla\cdot\boldsymbol{q}_h)_{\Omega_h} - \langle \frac{\partial}{\partial u_i}(u_h - \widehat{u}_h), (\widehat{\boldsymbol{q}}_h - \boldsymbol{q}_h)\cdot\boldsymbol{n} \rangle_{\partial\Omega_h} - \langle \frac{\partial}{\partial u_i}\widehat{u}_h, (\widehat{\boldsymbol{q}}_h - \boldsymbol{q}_h)\cdot\boldsymbol{n} \rangle_{\partial\Omega_h}\\
&\quad + (\frac{\partial}{\partial u_i}u_h, f(t))_{\Omega_h}\\
&= -(\frac{\partial}{\partial u_i}u_h, \nabla\cdot\boldsymbol{q}_h)_{\Omega_h} - \langle \frac{\partial}{\partial u_i}(u_h - \widehat{u}_h), (\widehat{\boldsymbol{q}}_h - \boldsymbol{q}_h)\cdot\boldsymbol{n} \rangle_{\partial\Omega_h} + \langle \frac{\partial}{\partial u_i}\widehat{u}_h, \frac{\beta}{\alpha}\widehat{u}_h - \frac{1}{\alpha}g(t) \rangle_{\Gamma}\\
&\quad + \langle \frac{\partial}{\partial u_i}\widehat{u}_h, \boldsymbol{q}_h\cdot\boldsymbol{n} \rangle_{\partial\Omega_h} + (\frac{\partial}{\partial u_i}u_h, f(t))_{\Omega_h} && \text{by (10d)},\\
&= -(\frac{\partial}{\partial u_i}u_h, \nabla\cdot\boldsymbol{q}_h)_{\Omega_h} + \langle \frac{\partial}{\partial u_i}\widehat{u}_h, \boldsymbol{q}_h\cdot\boldsymbol{n} \rangle_{\partial\Omega_h} - \langle \frac{\partial}{\partial u_i}(u_h - \widehat{u}_h), (\widehat{\boldsymbol{q}}_h - \boldsymbol{q}_h)\cdot\boldsymbol{n} \rangle_{\partial\Omega_h}\\
&\quad + \langle \frac{\partial}{\partial u_i}\widehat{u}_h, \frac{\beta}{\alpha}\widehat{u}_h - \frac{1}{\alpha}g(t) \rangle_{\Gamma} + (\frac{\partial}{\partial u_i}u_h, f(t))_{\Omega_h}
\end{aligned}$$

$$= -(\frac{\partial}{\partial u_i}u_h, \nabla \cdot \boldsymbol{q}_h)_{\Omega_h} + \langle \frac{\partial}{\partial u_i}\widehat{u}_h, \boldsymbol{q}_h \cdot \boldsymbol{n}\rangle_{\partial\Omega_h} - \langle \frac{\partial}{\partial u_i}(u_h - \widehat{u}_h), \tau(u_h - \widehat{u}_h)\rangle_{\partial\Omega_h}$$

$$+ \langle \frac{\partial}{\partial u_i}\widehat{u}_h, \frac{\beta}{\alpha}\widehat{u}_h - \frac{1}{\alpha}g(t)\rangle_\Gamma + (\frac{\partial}{\partial u_i}u_h, f(t))_{\Omega_h} \qquad \text{by (10e),}$$

$$= -(\frac{\partial}{\partial u_i}\boldsymbol{q}_h, \boldsymbol{q}_h)_{\Omega_h} - \langle \frac{\partial}{\partial u_i}(u_h - \widehat{u}_h), \tau(u_h - \widehat{u}_h)\rangle_{\partial\Omega_h}$$

$$+ \langle \frac{\partial}{\partial u_i}\widehat{u}_h, \frac{\beta}{\alpha}\widehat{u}_h - \frac{1}{\alpha}g(t)\rangle_\Gamma + (\frac{\partial}{\partial u_i}u_h, f(t))_{\Omega_h} \qquad \text{by (10c),}$$

$$= -\frac{\partial}{\partial u_i}H_h(u_h, v_h, t) = -\frac{\partial}{\partial \mathsf{q}_i}\mathcal{H}(\mathsf{p}, \mathsf{q}, t),$$

by the identity

$$\frac{\partial}{\partial u_i}H_h(u_h, v_h, t) = (\kappa^{-1}\frac{\partial}{\partial u_i}\boldsymbol{q}_h, \boldsymbol{q}_h)_{\Omega_h} + \langle \frac{\partial}{\partial u_i}(u_h - \widehat{u}_h), \tau(u_h - \widehat{u}_h)\rangle_{\partial\Omega_h}$$

$$- (f(t), \frac{\partial u_h}{\partial u_i})_{\Omega_h} - \langle (\frac{1}{\alpha})g(t), \frac{\partial\widehat{u}_h}{\partial u_i}\rangle_{\partial\Omega_h},$$

and the definition of $\mathcal{H}(\mathsf{p}, \mathsf{q}, t)$. This proves the first identity.

The second identity is simpler to prove. Indeed, we have

$$\dot{\mathsf{q}}_i = \dot{u}_i \qquad\qquad \text{by def. of } \mathsf{q}_i,$$

$$= v_i \qquad\qquad \text{by def. of } v_i,$$

$$= (\phi_i, v_h)_{\Omega_h} \qquad\qquad \text{by def. of } \phi_i,$$

$$= (\frac{\partial}{\partial v_i}v_h, v_h)_{\Omega_h}$$

$$= \frac{\partial}{\partial v_i}H_h(u_h, v_h, t) = \frac{\partial}{\partial \mathsf{p}_i}\mathcal{H}(\mathsf{p}, \mathsf{q}, t),$$

by the identity

$$\frac{\partial}{\partial v_i}H_h(u_h, v_h, t) = (\frac{\partial}{\partial v_i}v_h, v_h)_{\Omega_h},$$

and the definition of $\mathcal{H}(\mathsf{p}, \mathsf{q}, t)$. This completes the proof. $\square$

2.4. Post-processing

Next, we complete the presentation of the HDG methods by describing standard post-processing techniques for the displacement and velocity approximations.

2.4.1. Standard local post-processing of the displacement

We first consider a standard local post-processing for the displacement with the aim of improving the accuracy of the numerical approximation. Given the approximations $u_h, \boldsymbol{q}_h, \widehat{u}_h$ for a time T, we define, on every simplex $K \in \mathcal{T}_h$, a new approximate displacement $u_h^*|_K \in \mathcal{P}_{k+1}(K)$ to satisfy

$$\begin{aligned}(\nabla u_h^{n*}, \nabla w)_K &= (\boldsymbol{q}_h^n, \nabla w)_K, \quad \forall\, w \in \mathcal{P}_{k+1}(K),\\ (u_h^{n*}, 1)_K &= (u_h^n, 1)_K.\end{aligned} \tag{14}$$

The post-processing (14), requires us to solve a linear system whose size is the dimension of the space $\mathcal{P}_{k+1}(K)$.

2.4.2. Post-processing of the velocity

Given the velocity approximation v_h for a time T, in order to obtain a post-processed approximation v_h^*, we first compute an approximation $\boldsymbol{p}_h \in \mathcal{P}_k(K)$ to the velocity gradient $\boldsymbol{p} \equiv \nabla v$, by solving the following system

$$(\boldsymbol{p}_h, \boldsymbol{r})_{\Omega_h} - \langle \widehat{v}_h, \boldsymbol{r} \cdot \boldsymbol{n}\rangle_{\partial\Omega_h} = -(v_h, \nabla \cdot \boldsymbol{r})_{\Omega_h},$$

$$\langle \boldsymbol{p}_h \cdot \boldsymbol{n}, \mu\rangle_{\partial\Omega_h\backslash\Gamma} + \langle \tau\widehat{v}_h, \mu\rangle_{\partial\Omega_h\backslash\Gamma} + \langle \widehat{v}_h, \mu\rangle_\Gamma = \langle \tau v_h^n, \mu\rangle_{\partial\Omega_h\backslash\Gamma} + \langle \dot{g}(T), \rangle_\Gamma \tag{15}$$

for all $(\boldsymbol{v}, \mu) \in \boldsymbol{V}_h \times M_h$. We then find $v_h^{n*} \in \mathcal{P}_{k+1}(K)$ such that

$$(\nabla v_h^*, \nabla w)_K = (\boldsymbol{p}_h, \nabla w)_K, \quad \forall\, w \in \mathcal{P}_{k+1}(K),$$
$$(v_h^*, 1)_K = (v_h, 1)_K. \tag{16}$$

This post-processing step is similar to (14). The post-processing of the velocity is more expensive than that of the displacement because it requires the solution of the global system (15).

Note that (15) only works for the boundary condition $u = g$ on Γ.

2.5. Error estimates

We end this Section by recalling some convergence properties of the semidiscrete method just introduced. To do this, we use the fact that the semi-discrete HDG formulation defined in (10) is equivalent to the semi-discrete formulation introduced in [14], with the extra velocity variable in our case. Therefore, our formulation inherits the convergence properties proved in [14]. We state these convergence results and refer to [14] for their proof, see Theorem 2.3 and Corollary 2.4 therein. Note that the theoretical results in [14] only apply to the displacement post-processing. There is not theoretical result for the post-processing of the velocity only, as we see in Section 4, numerical evidence.

Theorem 2. *Suppose that the initial data* $(u_h(0), v_h(0))$ *is defined by* (11) *and* (12). *If* $\ddot{u}(t) \in H^{k+1}(\Omega)$ *for all* $t \in [0, T]$, *then, there exists a constant* $C > 0$, *independent of* h, *such that*

$$\|u(T) - u_h(T)\|_{L^2(\Omega)} \leq Ch^{k+1},$$
$$\|\boldsymbol{q}(T) - \boldsymbol{q}_h(T)\|_{L^2(\Omega)} + \|v(T) - v_h(T)\|_{L^2(\Omega)} \leq Ch^{k+1}.$$

Moreover, consider the post-processing displacement u_h^* *defined in Section 2.4 for* $k \geq 1$, *and assume that the following regularity result holds: there exists a constant* $C > 0$ *such that*

$$\|\eta\|_{H^2(\Omega)} \leq C \|\nabla \cdot (\kappa \nabla \eta)\|_{L^2(\Omega)},$$

for all $\eta \in H_0^1(\Omega)$ *such that* $\nabla \cdot (\kappa \nabla \eta) \in L^2(\Omega)$. *Then,*

$$\|u(T) - u_h^*(T)\|_{L^2(\Omega)} \leq Ch^{k+2},$$

for a constant $C > 0$ *independent of* h. *Note that the constants in the errors estimates depend on* T, *the stabilization parameter* τ, *and the exact solution.*

Observe that Theorem 2 provides optimal error estimates of order $k + 1$ for the semi-discrete HDG approximations of the displacement, velocity, and negative gradient of the displacement, as well as, a superconvergent rate of order $k + 2$ for the error of the post-processed displacement approximation. In fact, motivated by this superconvergence, we seek high-order accurate symplectic time stepping schemes, matching the $k + 2$ order of the spatial discretization. With this aim, in the following section, we introduce fully discrete schemes based on symplectic diagonally implicit and explicit partitioned Runge–Kutta methods for temporal discretizations.

3. Symplectic Hamiltonian HDG methods

In this section, we exploit the Hamiltonian structure of the semi-discrete HDG scheme (10) by pairing it with symplectic time integrators. The main property of these methods is that they preserve the symplecticity of the flow of Hamiltonian systems, which implies some desirable conservation properties such as the conservation of a modified Hamiltonian. For thorough overviews of symplectic time integrators see [30] and [21]. In principle, there is no restriction in terms of what symplectic integrator we can use. As mentioned earlier, in order to achieve accuracy of h^{k+2}, we naturally seek time stepping schemes with the same order (Δt^{k+2}). This is one of our main criteria for choosing the symplectic Runge–Kutta formulae. A second criterion, is that Symplectic Runge–Kutta methods are constructed starting from methods with vanishing stability matrix (see (19)). Methods with this property preserve quadratic invariants (see [15]) and are proven to be symplectic [2]. In particular, since the discrete Hamiltonian is a quadratic first integral of the semidiscrete HDG scheme for the wave equation, symplectic Runge–Kutta methods applied to this problem give exact conservation of the discrete Hamiltonian.

We present implicit and explicit schemes. For an implicit approach, we implement Symplectic Diagonally Implicit Runge–Kutta methods in Section 3.1 and denote these schemes by HDG-SDIRK. For general Hamiltonian equations, a well-known result is that explicit Runge–Kutta methods are not symplectic [21]. However, for cases where the Hamiltonian function is separable, which is the case under consideration, it is possible to derive explicit symplectic integrators using partitioned Runge–Kutta methods. This resulting numerical method is called HDG-ESPRK. In addition, we also provide a table of the CFL_{L^2} condition of these schemes.

In the following subsections, we present these fully discrete schemes. In order to illustrate the implementation ideas, we present for each case a one step method. For the fully implicit scheme (HDG-SDIRK), we write down the symplectic midpoint rule, whilst for the fully explicit scheme (HDG-ESPRK), we show the symplectic Euler method. These two basic symplectic methods are widely known, and their properties has been studied and contrasted with their non-symplectic variants. See [21] for illustrations of these comparisons.

3.1. Implicit schemes: HDG-SDIRK methods

As a first example of symplectic diagonally implicit Runge–Kutta methods, we consider the implicit midpoint scheme. Let us denote $z(t) = (p(t), q(t))^t$ and $f(t, z) = (\partial\mathcal{H}(t, p, q)/\partial q, -\partial\mathcal{H}(t, p, q)/\partial p)^t$. Then, we rewrite the Hamiltonian system of Theorem 1 as follows

$$\frac{dz}{dt} = f(t, z). \tag{17}$$

For a given time level t^n, with time step Δt^n, the implicit midpoint scheme for (17) reads as follows

$$z^{n+1} = z^n + \Delta t^n f(t^n + \frac{\Delta t^n}{2}, \frac{z^{n+1} + z^n}{2}),$$

for $z^n = z(t^n)$. Now we apply it to our scheme. Assume that we know the values of $u_h^n = u_h(t^n)$, $v_h^n = v_h(t^n)$, $\boldsymbol{q}_h^n = \boldsymbol{q}_h(t^n)$ and $\widehat{u}_h^n = \widehat{u}_h(t^n)$. Then, $u_h^{n+1}, v_h^{n+1}, \boldsymbol{q}_h^{n+1}, \widehat{u}_h^{n+1}$ are determined by the solution of the system

$$(u_h^{n+1}, w)_{\Omega_h} - \frac{\Delta t^n}{2}(v_h^{n+1}, w)_{\Omega_h} = (u_h^n, w)_{\Omega_h} + \frac{\Delta t^n}{2}(v_h^n, w)_{\Omega_h},$$

$$(v_h^{n+1}, w)_{\Omega_h} - \frac{\Delta t^n}{2}\left((\boldsymbol{q}_h^{n+1}, \nabla w)_{\Omega_h} - \langle\widehat{\boldsymbol{q}}_h^{n+1} \cdot \boldsymbol{n}, w\rangle_{\partial\Omega_h}\right) = (v_h^n, w)_{\Omega_h} + \frac{\Delta t^n}{2}\left((\boldsymbol{q}_h^n, \nabla w)_{\Omega_h} - \langle\widehat{\boldsymbol{q}}_h^n \cdot \boldsymbol{n}, w\rangle_{\partial\Omega_h}\right)$$

$$+ \Delta t^n(f(t^n + \frac{\Delta t^n}{2}), w)_{\Omega_h}$$

$$(\kappa^{-1}\boldsymbol{q}_h^{n+1}, \boldsymbol{r})_{\Omega_h} - (u_h^{n+1}, \nabla \cdot \boldsymbol{r})_{\Omega_h} + \langle\widehat{u}_h^{n+1}, \boldsymbol{r} \cdot \boldsymbol{n}\rangle_{\partial\Omega_h} = 0$$

$$\langle\widehat{\boldsymbol{q}}_h^{n+1} \cdot \boldsymbol{n}, \mu\rangle_{\partial\Omega_h\backslash\Gamma} = \langle\alpha\widehat{\boldsymbol{q}}_h^{n+1} \cdot \boldsymbol{n} - \beta\widehat{u}_h^{n+1} + g(t^{n+1}), \mu\rangle_\Gamma$$

$$\widehat{\boldsymbol{q}}_h^{n+1} \cdot \boldsymbol{n} = \boldsymbol{q}_h^{n+1} \cdot \boldsymbol{n} + \tau(u_h^{n+1} - \widehat{u}_h^{n+1}),$$

for $w \in W_h$, $\boldsymbol{r} \in \boldsymbol{V}_h$, and $\mu \in M_h$. The structure of the higher-order schemes described next is the same as the one above.

We now review the diagonally implicit Runge–Kutta schemes. The s-stage Diagonally Implicit Runge–Kutta (DIRK) method for the ODE system (17) is the following

$$z^{n+1} = z^n + \Delta t^n \sum_{i=1}^s b_i f(t^n + c_i\Delta t^n, y_i), \tag{18a}$$

$$y_i - \Delta t^n a_{ii}f(y_i) = z^n + \Delta t^n \sum_{j=1}^{i-1} a_{ij}f(t^n + c_i\Delta t^n, y_j), \quad 1 \leq i \leq s, \tag{18b}$$

where the coefficients a_{ij}, b_i, c_i, for $i, j = 1, \ldots, s$, are given in the form of the following Butcher tableau:

$$
\begin{array}{cccc|c}
a_{11} & 0 & \ldots & 0 & c_1 \\
a_{21} & a_{22} & \ddots & \vdots & c_2 \\
\vdots & \vdots & \ddots & 0 & \vdots \\
a_{s1} & a_{s2} & \ldots & a_{ss} & c_s \\
\hline
b_1 & b_2 & \ldots & b_s &
\end{array}
$$

The properties of a DIRK scheme (simplecticity, consistency, accuracy, and stability) are completely determined by the parameters b_j, a_{ij}. We are particularly interested in the class of symplectic DIRK schemes. A characterization of these schemes (see [21]) is given by the following equation for the coefficients

$$b_ib_j - b_ia_{ij} - b_ja_{ij} = 0, \quad 1 \leq i, j \leq s. \tag{19}$$

This formula yields, in the case of DIRK schemes, to Butcher tableaux of the form:

$$
\begin{array}{cccc|c}
b_1/2 & 0 & \ldots & 0 & b_1/2 \\
b_1 & b_2/2 & \ddots & \vdots & b_1 + b_2/2 \\
\vdots & \vdots & \ddots & 0 & \vdots \\
b_1 & b_2 & \ldots & b_s/2 & \sum_{i=1}^{s-1} b_i + b_s/2 \\
\hline
b_1 & b_2 & \ldots & b_s &
\end{array}
$$

Algorithm 1: HDG-SDIRK.

    Input : $(u_h^n, v_h^n, \boldsymbol{q}_h^n, \widehat{u}_h^n)$
    Output: $(u_h^{n+1}, v_h^{n+1}, \boldsymbol{q}_h^{n+1}, \widehat{u}_h^{n+1})$
1 Initialize $(u_h^{n+1}, v_h^{n+1}, \boldsymbol{q}_h^{n+1}, \widehat{u}_h^{n+1}) \leftarrow (u_h^n, v_h^n, \boldsymbol{q}_h^n, \widehat{u}_h^n)$;
2 **for** $i = 1$ *to* s **do**
3 $\tilde{u}_h^{n,i} \leftarrow d_{ii} u_h^n - \sum_{j=1}^{i-1} d_{ij}(u_h^{n,j} - u_h^n)$;
4 $\tilde{v}_h^{n,i} \leftarrow d_{ii} v_h^n - \sum_{j=1}^{i-1} d_{ij}(v_h^{n,j} - u_h^n)$;
5 $(u_h^{n,i}, v_h^{n,i}, \boldsymbol{q}_h^{n,i}, \widehat{u}_h^{n,i}) \leftarrow$ Solve system (21) for $(\tilde{u}_h^{n,i}, \tilde{v}_h^{n,i})$;
6 $u_h^{n+1} \leftarrow u_h^{n+1} + b_i \sum_{j=1}^{i} d_{ij}(u_h^{n,j} - u_h^n)$;
7 $v_h^{n+1} \leftarrow v_h^{n+1} + b_i \sum_{j=1}^{i} d_{ij}(v_h^{n,j} - u_h^n)$;
8 $\boldsymbol{q}_h^{n+1} \leftarrow \boldsymbol{q}_h^{n+1} + b_i \sum_{j=1}^{i} d_{ij}(\boldsymbol{q}_h^{n,j} - \boldsymbol{q}_h^n)$;
9 $\widehat{u}_h^{n+1} = \widehat{u}_h^{n+1} + b_i \sum_{j=1}^{i} d_{ij}(\widehat{u}_h^{n,j} - \widehat{u}_h^n)$;
10 **end**
11 return $(u_h^{n+1}, v_h^{n+1}, \boldsymbol{q}_h^{n+1}, \widehat{u}_h^{n+1})$

From the implementation viewpoint, it is convenient to rewrite the DIRK scheme (18) into the following system:

$$z^{n+1} = z^n + \sum_{i=1}^{s} b_i \sum_{j=1}^{i} d_{ij}(y_j - z^n) \tag{20a}$$

$$d_{ii} y_i - \Delta t^n f(y_i) = d_{ii} z^n - \sum_{j=1}^{i-1} d_{ij}(y_j - z^n), \quad 1 \le i \le s. \tag{20b}$$

Here d_{ij} is the inverse of the matrix a_{ij}. Concretely, system (20b) is written as follows

$$d_{ii}(u_h^{n,i}, w)_{\Omega_h} - \Delta t^n (v_h^{n,i}, w)_{\Omega_h} = (\tilde{u}_h^i, w)_{\Omega_h}$$

$$d_{ii}(v_h^{n,i}, w)_{\Omega_h} - \Delta t^n \left((\boldsymbol{q}_h^{n,i}, \nabla w)_{\Omega_h} - \langle \widehat{\boldsymbol{q}}_h^{n,i} \cdot \boldsymbol{n}, w \rangle_{\partial \Omega_h} \right) = (\tilde{v}_h^i, w)_{\Omega_h} + \Delta t^n (f(t^n + c_i \Delta t^n), w)_{\Omega_h}$$

$$(\kappa^{-1} \boldsymbol{q}_h^{n,i}, \boldsymbol{r})_{\Omega_h} + \langle \widehat{u}_h^{n,i}, \boldsymbol{r} \cdot \boldsymbol{n} \rangle_{\partial \Omega_h} - (u_h^{n,i}, \nabla \cdot \boldsymbol{r})_{\Omega_h} = 0 \tag{21}$$

$$\langle \widehat{\boldsymbol{q}}_h^{n,i} \cdot \boldsymbol{n}, \mu \rangle_{\partial \Omega_h \setminus \Gamma} = \langle \alpha \widehat{\boldsymbol{q}}_h^{n,i} \cdot \boldsymbol{n} - \beta \widehat{u}_h^{n,i} + g(t^n + c_i \Delta t^n), \mu \rangle_{\Gamma}$$

$$\widehat{\boldsymbol{q}}_h^{n,i} \cdot \boldsymbol{n} = \boldsymbol{q}_h^{n,i} \cdot \boldsymbol{n} + \tau(u_h^{n,i} - \widehat{u}_h^{n,i}),$$

for all $w \in W_h$, $\boldsymbol{r} \in \boldsymbol{V}_h$, $\mu \in M_h$, and where

$$\tilde{u}_h^i = d_{ii} u_h^n - \sum_{j=1}^{i-1} d_{ij}(u_h^{n,j} - u_h^n), \quad \tilde{v}_h^i = d_{ii} v_h^n - \sum_{j=1}^{i-1} d_{ij}(v_h^{n,j} - v_h^n) \tag{22}$$

for $i = 1, \ldots, s$. Thus, the HDG-SDIRK method can be outlined as it is shown in Algorithm 1.

3.2. Explicit scheme: HDG-ESPRK methods

We now consider fully explicit schemes based on partitioned Runge–Kutta methods. Similarly to the previous section, we illustrate the schemes with a one-stage partitioned Runge–Kutta method, the symplectic Euler method. For a given time level t^n, with time step Δt^n, assume that we know the values of $u_h^n = u_h(t^n)$, $v_h^n = v_h(t^n)$, $\boldsymbol{q}_h^n = \boldsymbol{q}_h(t^n)$ and $\widehat{u}_h^n = \widehat{u}_h(t^n)$. Then, $u_h^{n+1}, v_h^{n+1}, \boldsymbol{q}_h^{n+1}, \widehat{u}_h^{n+1}$ are determined by the solution of the system

$$(v_h^{n+1}, w)_{\Omega_h} = (v_h^n, w)_{\Omega_h} + \Delta t^n \left((\boldsymbol{q}_h^n, \nabla w)_{\Omega_h} + \langle \widehat{\boldsymbol{q}}_h^n \cdot \boldsymbol{n}, w \rangle_{\partial \Omega_h} \right) - \Delta t^n (f(t^n), w)_{\Omega_h}$$

$$(u_h^{n+1}, w)_{\Omega_h} = (u_h^n, w)_{\Omega_h} + \Delta t^n (v_h^{n+1}, w)_{\Omega_h}$$

$$(\kappa^{-1} \boldsymbol{q}_h^{n+1}, \boldsymbol{r})_{\Omega_h} + \langle \widehat{u}_h^{n+1}, \boldsymbol{r} \cdot \boldsymbol{n} \rangle_{\partial \Omega_h} = (u_h^{n+1}, \nabla \cdot \boldsymbol{r})_{\Omega_h}$$

$$\langle \widehat{\boldsymbol{q}}_h^{n+1} \cdot \boldsymbol{n}, \mu \rangle_{\partial \Omega_h \setminus \Gamma} = \langle \alpha \widehat{\boldsymbol{q}}_h^{n+1} \cdot \boldsymbol{n} - \beta \widehat{u}_h^{n+1} g(t^n + \Delta t^n), \mu \rangle_{\Gamma}$$

We now consider s-stages partitioned Runge–Kutta methods applied to the Hamiltonian system of Theorem 1. These methods have the following form:

$$\mathsf{p}^{n+1} = \mathsf{p}^n + \sum_i b_i k_i, \qquad\qquad \mathsf{q}^{n+1} = \mathsf{q}^n + \sum_i \tilde{b}_i \tilde{k}_i$$

$$k_i = -\frac{\partial}{\partial \mathsf{q}} \mathcal{H}(t^n + c_i \Delta t^n, \mathsf{p}^{n,i}, \mathsf{q}^{n,i}), \qquad \tilde{k}_i = \frac{\partial}{\partial \mathsf{p}} \mathcal{H}(t^n + \tilde{c}_i \Delta t^n, \mathsf{p}^{n,i}, \mathsf{q}^{n,i}), \quad i = 1, \dots, s, \tag{23}$$

$$\mathsf{p}^{n,i} = \mathsf{p}^n + \Delta t \sum_{j=1}^{s} a_{ij} k_j, \qquad\qquad \mathsf{q}^{n,i} = \mathsf{q}^n + \Delta t^n \sum_{j}^{s} \tilde{a}_{ij} \tilde{k}_j, \qquad\qquad i = 1, \dots, s,$$

where the coefficients on the left, a_{ij}, b_j, and the coefficients on the right, $\tilde{a}_{ij}, \tilde{b}_j$, determine two distinct Runge–Kutta methods. In addition, under the assumption of separability of the Hamiltonian, the partitioned Runge–Kutta method (23) is symplectic if the coefficients satisfy

$$b_i \tilde{a}_{ij} + \tilde{b}_j a_{ij} - b_j \tilde{b}_j = 0, \quad i, j = 1, \dots, s. \tag{24}$$

We observe that, although symplectic Euler can be written as a partitioned Runge–Kutta method, it does not satisfy condition (24). More precisely, symplectic Euler does not preserve quadratic invariants. Now, using the structure of the partitioned Runge–Kutta method (23), it is possible to devise fully explicit schemes with combinations of, for example, diagonally implicit and explicit Runge–Kutta methods. Specifically, let us consider a diagonally implicit Runge–Kutta scheme with coefficients a_{ij}, b_j, and an explicit Runge–Kutta scheme with coefficients $\tilde{a}_{ij}, \tilde{b}_j$, i.e., these coefficients satisfy

$$a_{ij} = 0, \quad i < j, \qquad \text{and} \qquad \tilde{a}_{ij} = 0, \quad i \le j, \quad j = 1, \dots, s. \tag{25}$$

For this case, the symplecticity condition (24) becomes

$$a_{ij} = b_j, \, i \ge j, \quad \text{and} \quad \tilde{a}_{ij} = \tilde{b}_j, \, i > j, \quad j = 1, \dots, s. \tag{26}$$

Thus, the Butcher tableaux associated with these schemes have the following structure

$$
\begin{array}{cccc|c}
b_1 & 0 & \dots & 0 & b_1/2 \\
 & & & \vdots & \vdots \\
b_1 & b_2 & \ddots & \vdots & b_1 + b_2 \\
\vdots & \vdots & \ddots & 0 & \vdots \\
b_1 & b_2 & \dots & b_s & \sum_{i=1}^{s} b_i \\
\hline
b_1 & b_2 & \dots & b_s &
\end{array}
\qquad
\begin{array}{ccccc|c}
0 & 0 & \dots & & 0 & 0 \\
\tilde{b}_1 & 0 & \ddots & & \vdots & \tilde{b}_1 \\
\tilde{b}_2 & \tilde{b}_2 & \ddots & & & \tilde{b}_1 + \tilde{b}_2 \\
\vdots & \vdots & \ddots & 0 & 0 & \vdots \\
\tilde{b}_1 & \tilde{b}_2 & \dots & \tilde{b}_{s-1} & 0 & \sum_{i=1}^{s-1} \tilde{b}_i \\
\hline
\tilde{b}_1 & \tilde{b}_2 & \dots & \tilde{b}_{s-1} & \tilde{b}_s &
\end{array}
$$

We now discuss in more detail the implementation of these methods to the HDG semi-discrete scheme (10). Observe that, considering the symplecticity condition (26) (equivalently the structure of the coefficients given in the table above), the symplectic partitioned Runge–Kutta scheme reads as follows:

$$\mathsf{p}^{n,i} = \mathsf{p}^n + \Delta t \sum_{j=1}^{i} b_{ij} k_j, \qquad\qquad \mathsf{q}^{n,i} = \mathsf{q}^n + \Delta t^n \sum_{j}^{i-1} \tilde{b}_{ij} \tilde{k}_j,$$

$$k_i = -\frac{\partial}{\partial \mathsf{q}} \mathcal{H}(t^n + c_i \Delta t^n, \mathsf{q}^{n,i}), \qquad \tilde{k}_i = \frac{\partial}{\partial \mathsf{p}} \mathcal{H}(t^n + c_i \Delta t^n, \mathsf{p}^{n,i}),$$

for $i = 1, \dots, s$, and hence obtaining $\mathsf{p}^{n+1} = \mathsf{p}^{n,s}$ and $\mathsf{q}^{n+1} = \mathsf{q}^{n,s}$. The scheme then is fully explicit, and in terms of our HDG method is formulated as follows:

$$(v_h^{n,i}, w)_{\Omega_h} = (v_h^{n,i-1}, w)_{\Omega_h} + b_i \Delta t^n \left((q_h^{n,i-1}, \nabla w)_{\Omega_h} + \langle \widehat{q}_h^{n,i-1} \cdot \boldsymbol{n}, w \rangle_{\partial \Omega_h} \right) - \Delta t^n b_i (f(t^n + c_i \Delta t^n), w)_{\Omega_h} \tag{27}$$

$$(u_h^{n,i}, w)_{\Omega_h} = (u_h^{n,i-1}, w)_{\Omega_h} + \tilde{b}_i \Delta t^n (v_h^{n,i}, w)_{\Omega_h} \tag{28}$$

Observe that, although the scheme is explicit for $v_h^{n,i}$ and $u_h^{n,i}$, we still need to solve for $q_h^{n,i}$ and $\widehat{u}_h^{n,i}$ in terms of $u_h^{n,i}$, in order to compute the next stage. In fact, this dependence is given by equations (10c), (10d) and (10e). Therefore, in order to implement the HDG-ESPRK we need to solve for a given u_h the following system for q_h and $\widehat{u}_h^{n,i}$

$$(\kappa^{-1} q_h^{n,i}, r)_{\Omega_h} + \langle \widehat{u}_h^{n,i}, r \cdot \boldsymbol{n} \rangle_{\partial \Omega_h} = (u_h^{n,i}, \nabla \cdot r)_{\Omega_h}$$

$$\langle q_h^{n,i} \cdot \boldsymbol{n} - \tau \widehat{u}_h^{n,i}, \mu \rangle_{\partial \Omega_h \backslash \Gamma} - \langle \alpha(q_h^{n,i} \cdot \boldsymbol{n} - \tau \widehat{u}_h^{n,i}) - \beta \widehat{u}_h^{n,i}, \mu \rangle_\Gamma = \langle \alpha \tau u_h^{n,i} + g(t^n + \tilde{c}_i \Delta t^n), \mu \rangle_\Gamma \tag{29}$$

for all $r \in \boldsymbol{V}_h$ and $\mu \in M_h$. Only once $q_h^{n,i}$ and $\widehat{u}_h^{n,i}$ are computed, we can proceed to the next stage. Observe that this systems is time independent (left-hand side), therefore it can be solved faster than the implicit scheme, using LU decomposition for

Algorithm 2: HDG-ESPRK.

Input : $(u_h^n, v_h^n, \boldsymbol{q}_h^n, \widehat{u}_h^n)$
Output: $(u_h^{n+1}, v_h^{n+1}, \boldsymbol{q}_h^{n+1}, \widehat{u}_h^{n+1})$

1 Initialize $(u_h^{n,1}, v_h^{n,0}, \boldsymbol{q}_h^{n,1}, \widehat{u}_h^{n,1}) \leftarrow (u_h^n, v_h^n, \boldsymbol{q}_h^n, \widehat{u}_h^n)$;
2 **for** $i = 1$ *to* s **do**
3 $\quad$ $v_h^{n,i} \leftarrow$ Solve (27) given $(v_h^{n,i-1}, \boldsymbol{q}_h^{n,i}, \widehat{u}_h^{n,i}, b_i)$;
4 $\quad$ $u_h^{n,i+1} \leftarrow u_h^{n,i} + \Delta t^n \tilde{b}_{i+1} v_h^{n,i}$;
5 $\quad$ $(\boldsymbol{q}_h^{n,i+1}, \widehat{u}_h^{n,i+1}) \leftarrow$ Solve system (29) given $(u_h^{n,i})$;
6 **end**
7 return $(u_h^{n,s+1}, v_h^{n,s}, \boldsymbol{q}_h^{n,s+1}, \widehat{u}_h^{n,s+1})$

Table 1
CFL$_{L^2}$ numbers for methods HDG-ESPRK, using polynomials of order k in the HDG discretization and the ESPRK schemes of order ν detailed in Appendix A.2.

$\nu\backslash k$	0	1	2	3	4
1		0.5764	0.2577	0.1531	0.1025
3		0.7217	0.2131	0.1919	0.1284
4		0.8404	0.3758	0.2232	0.1493
5		0.8838	0.3949	0.2345	0.1569
6		1.7709	0.7921	0.4705	0.3101

example. An alternative to avoid this difficulty would be to use a local space discretization such as a Local DG method. We see below in Section 5.1, that this method indeed is a suitable candidate since it also preserves the Hamiltonian structure of the wave equation. We outline the implementation of the HDG-ESPRK fully discrete scheme in Algorithm 2.

Furthermore, we present in Table 1 with CFL$_{L^2}$ numbers for the explicit family of methods HDG-ESPRK.

4. Numerical experiments

In this section, we show numerical experiments illustrating the convergence properties of the implicit and explicit Hamiltonian HDG schemes, HDG-SDIRK and HDG-ESPRK, respectively. We specify in our methods the polynomial order k of the HDG scheme and the order ν of the Runge–Kutta method, by means of the notation HDG(k)-SDIRK(ν) and HDG(k)-ESPRK(ν). The coefficients of the respective Runge–Kutta methods used in our computations are presented in the appendix. As mentioned earlier, in order to observe the superconvergence properties of the post-processed approximations we need $\nu \geq k + 2$. We report error tables for the approximations u_h, v_h, $\boldsymbol{q}_h$, u_h^* and v_h^*, in which we compute the errors as the maximum over the time steps t^n of the L^2 errors of the numerical approximations, and their estimated orders of convergence (e.o.c). For instance, for the displacement approximation, we compute

$$\text{error}_h = \max_{t^n} \|u(t^n) - u_h^n\|_{L^2(\Omega)}.$$

In our computations, we use a mesh size $h = 2^{-l}$, and we report the value of l in the error tables.

We present two sets of experiments. In the first, we verify the convergence properties of the numerical schemes, whilst, in the second, we test the energy conservative properties of our scheme HDG-SDIRK comparing it with the dissipative HDG method, also based on DIRK formulae, presented in [26]; this dissipative HDG method is based on the velocity-stress formulation of the wave equation. We also illustrate the importance of using symplectic methods which preserve quadratic invariants by comparing the energies obtained by the symplectic Euler scheme, which does not preserve quadratic invariants, and the implicit midpoint scheme, which does.

4.1. Verification of the convergence properties

We present two numerical examples, in the one- and two-dimensional cases, verifying the expected convergence properties of the numerical schemes HDG-SDIRK and HDG-ESPRK.

Example 4.1. We consider the following exact solution of the acoustic wave equation (1) in one dimension,

$$u(t, x) = \frac{1}{\pi} \sin(\pi(x - \varepsilon)) \cos(\pi t), \quad x \in (0, 1), \, t \in (0, T_f],$$ (30)

with parameters $\kappa = 1$, $\alpha = 0$ and $\beta = 1$, i.e., with Dirichlet boundary conditions. We study the following cases:

a) Exact solution with $\varepsilon = 0$. We test the convergence properties of the schemes HDG(k)-SDIRK($k + 2$) and HDG(k)-ESPRK($k + 2$). We report in Tables 2 and 3, respectively, the L^2-errors and their estimated orders of convergence (e.o.c.) for the numerical approximations up to the final time $T_f = 1.0$. Here we use the initial condition given by (11). We

Table 2

Example 4.1: History of convergence of the numerical approximations of the wave equation with exact solution $u(t, x) = (1/\pi) \sin(\pi x) \cos(\pi t)$ by the schemes HDG(k)-SDIRK($k+2$). Computations were performed up to a final time $T_f = 1.0$ and with a time step $\Delta t = h$.

k	l	u_h		v_h		$\mathbf{q}_h$		u_h^*		v_h^*	
		error	e.o.c.	error	e.o.c.	error	e.o.c.	error	e.o.c.	error	e.o.c.
1	1	3.4e−02	–	1.7e−01	–	1.7e−01	–	3.0e−02	–	1.6e−01	–
	2	7.1e−03	2.27	2.2e−02	2.99	5.0e−02	1.75	6.3e−03	2.27	2.2e−02	2.90
	3	1.5e−03	2.28	4.3e−03	2.32	1.5e−02	1.79	6.0e−04	3.38	1.2e−03	4.21
	4	3.5e−04	2.05	1.1e−03	2.00	3.9e−03	1.88	7.6e−05	2.99	1.6e−04	2.85
	5	8.7e−05	2.02	2.7e−04	2.00	1.0e−03	1.94	9.9e−06	2.94	2.8e−05	2.55
	6	2.2e−05	2.00	6.9e−05	1.98	2.6e−04	1.97	1.3e−06	2.97	4.3e−06	2.69
	7	5.4e−06	2.00	1.7e−05	2.00	6.6e−05	1.98	1.6e−07	2.98	6.0e−07	2.86
	8	1.4e−06	2.00	4.3e−06	2.00	1.7e−05	1.99	2.0e−08	2.99	7.8e−08	2.93
2	1	3.7e−02	–	2.3e−01	–	1.2e−01	–	3.7e−02	–	2.3e−01	–
	2	6.1e−03	2.60	3.6e−02	2.70	1.9e−02	2.59	6.1e−03	2.60	3.6e−02	2.70
	3	5.7e−04	3.44	3.1e−03	3.53	1.8e−03	3.44	5.7e−04	3.44	3.1e−03	3.53
	4	3.9e−05	3.86	2.1e−04	3.87	1.3e−04	3.83	3.9e−05	3.87	2.1e−04	3.87
	5	2.5e−06	3.95	1.4e−05	3.96	9.1e−06	3.78	2.5e−06	3.96	1.4e−05	3.96
	6	1.6e−07	3.95	8.5e−07	3.99	1.0e−06	3.17	1.6e−07	3.99	8.5e−07	3.99
	7	1.2e−08	3.75	5.3e−08	4.00	1.3e−07	2.99	9.8e−09	4.00	5.3e−08	4.00
	8	1.4e−09	3.11	4.4e−09	3.60	1.6e−08	3.00	6.1e−10	4.01	3.3e−09	4.00
3	1	7.1e−03	–	4.5e−02	–	2.2e−02	–	7.1e−03	–	4.5e−02	–
	2	4.6e−04	3.93	2.7e−03	4.02	1.5e−03	3.93	4.6e−04	3.93	2.7e−03	4.02
	3	1.4e−05	5.08	7.5e−05	5.20	4.3e−05	5.08	1.4e−05	5.08	7.5e−05	5.20
	4	2.5e−07	5.75	1.4e−06	5.76	9.0e−07	5.58	2.5e−07	5.76	1.4e−06	5.76
	5	4.9e−09	5.69	2.2e−08	5.94	4.8e−08	4.24	4.1e−09	5.93	2.2e−08	5.94
	6	2.8e−10	4.16	8.6e−10	4.70	3.0e−09	3.99	6.5e−11	5.98	3.5e−10	5.98
	7	1.7e−11	4.00	5.4e−11	4.00	1.9e−10	3.99	1.6e−12	5.32	5.6e−12	5.98
4	1	2.8e−03	–	1.8e−02	–	8.9e−03	–	2.8e−03	–	1.8e−02	–
	2	1.2e−04	4.61	6.9e−04	4.70	3.7e−04	4.61	1.2e−04	4.61	6.9e−04	4.70
	3	2.7e−06	5.45	1.5e−05	5.57	8.4e−06	5.45	2.7e−06	5.45	1.5e−05	5.57
	4	4.5e−08	5.88	2.5e−07	5.88	1.4e−07	5.88	4.5e−08	5.88	2.5e−07	5.88
	5	7.2e−10	5.97	3.9e−09	5.97	2.3e−09	5.97	7.2e−10	5.97	3.9e−09	5.97
	6	1.1e−11	6.00	6.1e−11	6.00	3.6e−11	5.99	1.1e−11	6.06	6.1e−11	6.00
	7	1.1e−13	6.67	1.6e−12	5.22	2.3e−12	3.94	4.8e−12	1.17	1.5e−11	2.00

Table 3

Example 4.1: History of convergence of numerical approximations of the wave equation with exact solution $u(t, x) = (1/\pi) \sin(\pi x) \cos(\pi t)$ by the schemes HDG(k)-ESPRK($k+2$). Computations were performed up to a final time $T_f = 1.0$.

k	l	u_h		v_h		$\mathbf{q}_h$		u_h^*		v_h^*	
		error	e.o.c.	error	e.o.c.	error	e.o.c.	error	e.o.c.	error	e.o.c.
1	1	3.0e−02	–	8.5e−02	–	1.6e−01	–	2.5e−02	–	8.5e−02	–
	2	6.4e−03	2.23	1.9e−02	2.20	5.0e−02	1.66	3.9e−03	2.67	1.5e−02	2.53
	3	1.5e−03	2.13	4.5e−03	2.04	1.5e−02	1.79	5.6e−04	2.79	2.2e−03	2.74
	4	3.5e−04	2.05	1.1e−03	2.04	3.9e−03	1.88	7.6e−05	2.88	3.1e−04	2.85
	5	8.7e−05	2.02	2.8e−04	2.00	1.0e−03	1.94	9.9e−06	2.94	4.0e−05	2.93
	6	2.2e−05	2.00	6.9e−05	2.00	2.6e−04	1.97	1.3e−06	2.97	5.1e−06	2.97
	7	5.5e−06	2.00	1.7e−05	2.00	6.6e−05	1.98	1.6e−07	2.98	6.5e−07	2.98
	8	1.4e−06	2.00	4.3e−06	2.00	1.7e−05	1.99	2.0e−08	2.99	8.2e−08	2.99
2	1	3.1e−03	–	1.1e−02	–	2.3e−02	–	1.7e−03	–	6.1e−03	–
	2	3.7e−04	3.04	1.2e−03	3.20	3.5e−03	2.74	1.3e−04	3.73	4.2e−04	3.88
	3	4.6e−05	3.02	1.4e−04	3.00	4.7e−04	2.87	9.0e−06	3.87	2.9e−05	3.83
	4	5.7e−06	3.01	1.8e−05	3.00	6.2e−05	2.93	5.9e−07	3.93	1.9e−06	3.95
	5	7.1e−07	3.00	2.2e−06	3.00	8.0e−06	2.96	3.8e−08	3.96	1.2e−07	3.97
	6	8.9e−08	3.00	2.8e−07	3.00	1.0e−06	2.98	2.4e−09	3.98	7.6e−09	3.99
	7	1.1e−08	3.00	3.5e−08	2.99	1.3e−07	2.99	1.5e−10	3.99	4.8e−10	4.00
	8	1.4e−09	3.00	4.4e−09	3.00	1.6e−08	3.00	1.3e−11	3.58	3.9e−11	3.61
3	1	2.9e−04	–	9.4e−04	–	2.4e−03	–	1.3e−04	–	4.5e−04	–
	2	1.8e−05	4.01	5.7e−05	4.04	1.7e−04	3.81	4.5e−06	4.80	1.4e−05	4.97
	3	1.1e−06	4.00	3.5e−06	4.01	1.2e−05	3.90	1.5e−07	4.91	4.8e−07	4.92
	4	7.0e−08	4.00	2.2e−07	3.99	7.5e−07	3.95	4.9e−09	4.95	1.6e−08	4.94
	5	4.4e−09	4.00	1.4e−08	4.01	4.8e−08	3.97	1.6e−10	4.97	4.9e−10	4.98
	6	2.8e−10	4.00	8.7e−10	3.99	3.0e−09	3.99	4.9e−12	4.98	1.6e−11	4.98
	7	1.7e−11	4.00	5.4e−11	4.00	1.9e−10	3.99	1.6e−12	1.59	5.2e−12	1.59
4	1	2.3e−05	–	7.1e−05	–	2.0e−04	–	8.0e−06	–	2.7e−05	–
	2	7.1e−07	5.00	2.2e−06	5.00	6.9e−06	4.86	1.4e−07	5.88	4.7e−07	5.86
	3	2.2e−08	5.00	7.0e−08	4.99	2.3e−07	4.92	2.3e−09	5.91	7.2e−09	6.01
	4	6.9e−10	5.00	2.2e−09	5.01	7.3e−09	4.96	3.6e−11	5.96	1.2e−10	5.97
	5	2.2e−11	5.00	6.8e−11	4.99	2.3e−10	4.98	6.3e−13	5.85	2.0e−12	5.83

Table 4

Example 4.1: History of convergence of the numerical approximations of the wave equation with exact solution $u(t,x) = (1/\pi)\sin(\pi x)\cos(\pi t)$ by the scheme HDG(1)-SDIRK(3), initializing with the L^2 projections and HDG-projections of the initial data. Computations were performed up to a final time $T_f = 1.0$ and with a time step $\Delta t = h/2$.

l	u_h		v_h		$\boldsymbol{q}_h$		u_h^*		v_h^*	
	error	e.o.c.	error	e.o.c.	error	e.o.c.	error	e.o.c.	error	e.o.c.
HDG(1)-DIRK(3), initial condition L^2 projection										
1	3.1e–02	–	2.4e–01	–	2.5e–01	–	2.8e–02	–	1.3e–01	–
2	6.4e–03	2.27	4.7e–02	2.33	8.3e–02	1.60	4.7e–03	2.59	2.5e–02	2.42
3	1.4e–03	2.22	1.1e–02	2.15	2.6e–02	1.65	4.5e–04	3.40	2.2e–03	3.52
4	3.9e–04	1.83	4.2e–03	1.34	7.6e–03	1.80	6.2e–05	2.85	3.0e–04	2.85
5	1.0e–04	1.93	1.4e–03	1.57	2.0e–03	1.94	8.1e–06	2.95	5.6e–05	2.44
6	2.5e–05	2.00	5.3e–04	1.43	5.1e–04	1.96	1.1e–06	2.82	1.0e–05	2.46
7	6.4e–06	1.99	1.8e–04	1.51	1.3e–04	1.98	1.5e–07	2.91	1.8e–06	2.50
HDG(1)-DIRK(3), initial condition HDG-projection										
1	3.0e–02	–	2.2e–01	–	2.7e–01	–	3.1e–02	–	1.4e–01	–
2	5.6e–03	2.43	2.7e–02	3.01	6.9e–02	1.97	4.7e–03	2.74	2.3e–02	2.62
3	1.4e–03	2.03	4.4e–03	2.62	1.7e–02	2.00	2.9e–04	4.00	1.2e–03	4.31
4	3.5e–04	1.97	1.1e–03	1.96	4.3e–03	2.00	3.5e–05	3.05	1.4e–04	3.07
5	8.7e–05	2.01	2.8e–04	2.05	1.1e–03	2.00	5.5e–06	2.70	2.6e–05	2.42
6	2.2e–05	2.00	6.9e–05	1.99	2.7e–04	2.00	8.3e–07	2.71	4.3e–06	2.61
7	5.4e–06	2.00	1.7e–05	2.01	6.7e–05	2.00	1.1e–07	2.86	5.9e–07	2.84

Table 5

Example 4.1: History of convergence of the numerical approximations of the wave equation with exact solution $u(t,x) = (1/\pi)\sin(\pi x)\cos(\pi t)$ by the scheme HDG(1)-ESPRK(3), initializing with the L^2 projections and HDG-projections of the initial data. Computations were performed up to a final time $T_f = 1.0$ and with a time step $\Delta t = h/2$.

l	u_h		v_h		$\boldsymbol{q}_h$		u_h^*		v_h^*	
	error	e.o.c.	error	e.o.c.	error	e.o.c.	error	e.o.c.	error	e.o.c.
HDG(1)-ESPRK(3), initial condition L^2 projection										
1	3.9e–02	–	3.0e–01	–	1.9e–01	–	3.7e–02	–	2.9e–01	–
2	1.1e–02	1.81	4.8e–02	2.63	5.2e–02	1.85	1.1e–02	1.75	4.5e–02	2.67
3	2.9e–03	1.95	1.4e–02	1.76	1.5e–02	1.83	2.8e–03	1.98	1.0e–02	2.14
4	7.1e–04	2.03	4.5e–03	1.65	4.0e–03	1.85	7.0e–04	2.01	2.5e–03	2.01
5	1.7e–04	2.02	1.5e–03	1.56	1.0e–03	1.95	1.7e–04	2.03	6.0e–04	2.10
6	4.3e–05	2.01	5.3e–04	1.55	2.6e–04	1.98	4.2e–05	2.02	1.4e–04	2.06
7	1.1e–05	2.01	1.9e–04	1.50	6.7e–05	1.99	1.1e–05	2.01	3.5e–05	2.04
HDG(1)-ESPRK(3), initial condition HDG projection										
1	7.0e–02	–	7.8e–01	–	3.0e–01	–	3.6e–02	–	5.0e–01	–
2	6.0e–03	3.55	2.5e–02	4.99	6.9e–02	2.12	2.3e–03	3.99	1.3e–02	5.28
3	1.4e–03	2.11	5.2e–03	2.24	1.7e–02	2.00	3.6e–04	2.66	2.1e–03	2.62
4	3.5e–04	1.98	1.1e–03	2.19	4.3e–03	2.00	5.2e–05	2.81	3.0e–04	2.78
5	8.7e–05	2.00	2.8e–04	2.04	1.1e–03	2.00	6.9e–06	2.90	4.0e–05	2.94
6	2.2e–05	2.00	6.9e–05	2.01	2.7e–04	2.00	8.9e–07	2.95	5.1e–06	2.95
7	5.4e–06	2.00	1.7e–05	2.01	6.7e–05	2.00	1.1e–07	2.97	6.5e–07	2.98

observe optimal rates of convergence $k+1$ for the approximations of the displacement u_h, velocity v_h and negative gradient $\boldsymbol{q}_h$, and a rate of convergence $k+2$ for the post-processed approximations of the displacement u_h^* and velocity v_h^*.

b) Exact solution with $\varepsilon = 0$. We study the effect of other initial conditions on our numerical schemes. We first consider the L^2-projection of the initial data and then the HDG-projection of the initial data. We compute the errors of the approximations of the schemes HDG(1)-SDIRK(3) and HDG(1)-ESPRK(3). These results are reported in Tables 4 and 5, respectively. We observe that when the L^2-projection is used the HDG(1)-SDIRK(3) scheme exhibits suboptimal convergence of order 1.5 and 2.5 for the velocity and the post-processed velocity, whereas when the HDG-projection is used the results are optimal. For the scheme HDG(1)-ESPRK(3) with the L^2-projection of the initial data we observe not only the same suboptimal rate of 1.5 of the velocity approximation, but also sub-optimal rate of 2 for the post-processed displacement and velocity. The HDG projection gives optimal approximations for this scheme as well.

c) Exact solution $\varepsilon = 0.5$. We study the effect of time-dependent boundary conditions (non-autonomous dynamics). Considering piecewise linear approximations, we compute the errors by the schemes HDG(1)-DIRK(3) and HDG(1)-ESPRK(3), and report them in Tables 6 and 7, first using the time step $\Delta t = h$ and then $\Delta t = h^{3/2}$. For both schemes we observe suboptimal results (particularly on the velocity approximation) when $\Delta t = h$ is used. For the second case, $\Delta t = h^{3/2}$, the convergence is recovered, showing the convergence properties of the semi-discrete scheme.

Table 6

Example 4.1: History of convergence of the numerical approximations of the wave equation with exact solution $u(t,x) = (1/\pi)\sin(\pi(x+1/2))\cos(\pi t)$ by the scheme HDG(1)-SDIRK(3). Computations were performed up to a final time $T_f = 1.0$ and with a time steps $\Delta t = h$ and $\Delta t = h^{3/2}$.

l	u_h		v_h		$\boldsymbol{q}_h$		u_h^*		v_h^*	
	error	e.o.c.	error	e.o.c.	error	e.o.c.	error	e.o.c.	error	e.o.c.
HDG(1)-DIRK(3), $\Delta t = h$										
1	1.9e–01	–	6.8e–01	–	9.3e–01	–	2.0e–01	–	6.4e–01	–
2	5.1e–02	1.90	4.2e–01	0.70	6.1e–01	0.60	5.0e–02	1.96	3.7e–01	0.77
3	1.1e–02	2.25	1.6e–01	1.42	2.1e–01	1.57	1.1e–02	2.25	1.5e–01	1.29
4	1.8e–03	2.57	5.2e–02	1.60	8.2e–02	1.34	1.9e–03	2.44	5.4e–02	1.49
5	3.3e–04	2.47	1.7e–02	1.59	3.0e–02	1.46	3.3e–04	2.55	1.9e–02	1.53
6	6.1e–05	2.43	5.9e–03	1.55	1.1e–02	1.49	6.0e–05	2.46	6.6e–03	1.53
7	1.1e–05	2.42	2.0e–03	1.52	3.7e–03	1.50	1.1e–05	2.49	2.3e–03	1.52
HDG(1)-DIRK(3), $\Delta t = h^{3/2}$										
1	1.0e–01	–	7.2e–01	–	7.2e–01	–	9.5e–02	–	6.1e–01	–
2	1.2e–02	3.16	1.4e–01	2.32	1.6e–01	2.20	1.0e–02	3.23	1.4e–01	2.12
3	1.5e–03	2.96	1.7e–02	3.07	3.7e–02	2.09	1.0e–03	3.31	1.7e–02	3.07
4	3.6e–04	2.06	2.5e–03	2.79	7.8e–03	2.24	1.3e–04	3.03	2.6e–03	2.67
5	8.8e–05	2.03	3.2e–04	2.94	1.6e–03	2.29	1.6e–05	3.02	3.6e–04	2.87
6	2.2e–05	2.01	7.1e–05	2.18	3.4e–04	2.22	1.9e–06	3.04	4.7e–05	2.91
7	5.5e–06	2.00	1.7e–05	2.04	7.7e–05	2.15	2.3e–07	3.02	6.1e–06	2.97

Table 7

Example 4.1: History of convergence of the numerical approximations of the wave equation with exact solution $u(t,x) = (1/\pi)\sin(\pi(x+1/2))\cos(\pi t)$ by the scheme HDG(1)-ESPRK(3). Computations were performed up to a final time $T_f = 1.0$ and with a time steps $\Delta t = h$ and $\Delta t = h^{3/2}$.

l	u_h		v_h		$\boldsymbol{q}_h$		u_h^*		v_h^*	
	error	e.o.c.	error	e.o.c.	error	e.o.c.	error	e.o.c.	error	e.o.c.
HDG(1)-ESPRK(3), $\Delta t = h$										
1	3.0e–02	–	1.0e–01	–	1.6e–01	–	2.3e–02	–	9.9e–02	–
2	6.9e–03	2.14	2.3e–02	2.15	5.1e–02	1.63	4.7e–03	2.31	2.0e–02	2.33
3	1.5e–03	2.17	5.2e–03	2.13	1.5e–02	1.80	7.3e–04	2.69	3.4e–03	2.55
4	3.6e–04	2.09	1.3e–03	2.02	3.9e–03	1.88	1.0e–04	2.85	1.2e–03	1.55
5	8.8e–05	2.03	3.5e–04	1.88	1.0e–03	1.93	1.4e–05	2.90	3.5e–04	1.70
6	2.2e–05	2.01	1.1e–04	1.65	2.8e–04	1.87	1.8e–06	2.91	1.2e–04	1.52
7	5.5e–06	2.00	3.9e–05	1.51	7.9e–05	1.84	2.4e–07	2.90	4.3e–05	1.51
HDG(1)-ESPRK(3), $\Delta t = h^{3/2}$										
1	2.9e–02	–	1.1e–01	–	1.6e–01	–	2.4e–02	–	1.0e–01	–
2	7.1e–03	2.04	2.2e–02	2.34	5.3e–02	1.57	5.1e–03	2.24	1.7e–02	2.58
3	1.5e–03	2.20	4.8e–03	2.17	1.5e–02	1.84	7.7e–04	2.72	2.4e–03	2.81
4	3.6e–04	2.10	1.1e–03	2.09	4.0e–03	1.91	1.1e–04	2.86	3.3e–04	2.87
5	8.8e–05	2.03	2.8e–04	2.03	1.0e–03	1.95	1.4e–05	2.93	4.3e–05	2.92
6	2.2e–05	2.01	6.9e–05	2.01	2.6e–04	1.97	1.8e–06	2.97	5.5e–06	2.97
7	5.5e–06	2.00	1.7e–05	2.00	6.6e–05	1.98	2.2e–07	2.98	7.0e–07	2.98

Example 4.2. We consider the following exact solution of the two dimensional acoustic wave equation:

$$u(t,x,y) = \frac{1}{\sqrt{2}\pi}\sin(\pi x)\sin(\pi y)\cos(\sqrt{2}\pi t), \quad x,y \in (0,1)^2, \, t \in (0,T_f], \tag{31}$$

with parameters $\kappa = 1$, $\alpha = 0$ and $\beta = 1$, i.e., with Dirichlet boundary conditions. We report in Table 8 and 9 the errors and estimated orders of convergence of the approximations by the schemes HDG(k)-SDIRK($k+2$) and HDG(k)-ESPRK($k+2$), respectively, for $k = 1,2,3,4$. We observe optimal convergence as in the one dimensional case.

4.2. Comparison with dissipative HDG methods and verification of energy conservation properties

The purpose of the following experiments is to compare the energy-conservative schemes presented in this paper with the dissipative HDG schemes introduced in [26]. Notice that these schemes have also optimal convergence properties and utilize DIRK formulae for time integration. Thus, in the examples below, we use the same SDIRK method for both schemes. We consider three examples of traveling wave solutions on periodic domains, two one dimensional and one two dimensional. In the first example, we set the exact solution to be a sinusoidal signal, first with low frequency and then with a higher frequency. In the second example, we consider an impulse solution to observe the long time behavior of the approximations. Finally, in the third example we consider two impulse solutions traveling in perpendicular directions. In order to diminish the dispersive effects in the numerical approximations, we use Runge–Kutta schemes of order 5.

Table 8

Example 4.2: History of convergence of the numerical approximations of the wave equation with exact solution $u(t, x, y) = (1/(\sqrt{2}\pi)) \sin(\pi x) \sin(\pi y) \cos(\sqrt{2}\pi t)$ by the schemes HDG(k)-SDIRK($k + 2$). Computations were performed up to a final time $T_f = 1.0$ and with a time step $\Delta t = h$.

k	l	u_h error	e.o.c.	v_h error	e.o.c.	q_h error	e.o.c.	u_h^* error	e.o.c.	v_h^* error	e.o.c.
1	1	1.2e–01	–	8.8e–01	–	5.2e–01	–	1.2e–01	–	8.8e–01	–
	2	6.9e–02	0.78	3.0e–01	1.56	3.1e–01	0.77	6.9e–02	0.78	3.0e–01	1.56
	3	1.5e–02	2.24	5.1e–02	2.54	6.5e–02	2.24	1.5e–02	2.24	5.1e–02	2.54
	4	1.4e–03	3.42	4.7e–03	3.46	6.1e–03	3.42	1.4e–03	3.42	4.7e–03	3.46
	5	9.4e–05	3.86	3.3e–04	3.84	4.3e–04	3.82	9.3e–05	3.87	3.2e–04	3.86
2	1	1.0e–03	–	4.8e–03	–	9.8e–03	–	4.3e–04	–	2.2e–03	–
	2	1.3e–04	3.02	5.7e–04	3.09	1.4e–03	2.81	3.2e–05	3.75	1.4e–04	3.95
	3	1.6e–05	3.01	6.9e–05	3.05	1.9e–04	2.92	2.1e–06	3.90	9.3e–06	3.97
	4	2.0e–06	3.01	8.5e–06	3.01	2.4e–05	2.96	1.4e–07	3.95	5.8e–07	4.00
	5	2.5e–07	3.00	1.1e–06	2.99	3.0e–06	2.98	8.8e–09	3.98	3.8e–08	3.93
3	1	1.1e–04	–	4.8e–04	–	1.1e–03	–	3.8e–05	–	1.8e–04	–
	2	6.8e–06	4.00	2.9e–05	4.05	8.0e–05	3.85	1.3e–06	4.85	5.4e–06	5.09
	3	4.2e–07	4.00	1.8e–06	4.00	5.2e–06	3.93	4.3e–08	4.93	1.8e–07	4.89
	4	2.6e–08	4.00	1.1e–07	3.99	3.4e–07	3.97	1.4e–09	4.97	6.0e–09	4.93
	5	1.7e–09	4.00	7.1e–09	4.00	2.1e–08	3.98	4.3e–11	4.98	1.9e–10	5.00
4	1	8.0e–06	–	3.5e–05	–	8.7e–05	–	1.9e–06	–	8.9e–06	–
	2	2.5e–07	4.98	1.1e–06	5.02	3.0e–06	4.87	3.3e–08	5.82	1.4e–07	5.99
	3	7.9e–09	4.99	3.4e–08	4.99	9.7e–08	4.94	5.4e–10	5.94	2.4e–09	5.89
	4	2.5e–10	5.00	1.1e–09	5.00	3.1e–09	4.98	8.7e–12	5.97	3.7e–11	6.01
	5	7.8e–12	5.00	3.4e–11	4.98	9.7e–11	4.99	6.5e–13	3.74	6.4e–12	2.52

Table 9

Example 4.2: History of convergence of the numerical approximations of the wave equation with exact solution $u(t, x, y) = (1/(\sqrt{2}\pi)) \sin(\pi x) \sin(\pi y) \cos(\sqrt{2}\pi t)$ by the schemes HDG(k)-ESPRK($k + 2$). Computations were performed up to a final time $T_f = 1.0$.

k	l	u_h error	e.o.c.	v_h error	e.o.c.	q_h error	e.o.c.	u_h^* error	e.o.c.	v_h^* error	e.o.c.
1	1	1.2e–02	–	4.6e–02	–	7.7e–02	–	1.2e–02	–	3.7e–02	–
	2	2.3e–03	2.38	9.2e–03	2.30	2.3e–02	1.75	2.1e–03	2.53	2.4e–03	3.98
	3	5.5e–04	2.10	2.3e–03	2.03	6.3e–03	1.87	3.0e–04	2.81	3.8e–04	2.63
	4	1.3e–04	2.04	5.6e–04	2.01	1.7e–03	1.93	4.0e–05	2.91	5.0e–05	2.93
	5	3.3e–05	2.01	1.4e–04	1.99	4.2e–04	1.97	5.1e–06	2.95	6.5e–06	2.95
2	1	1.0e–03	–	4.8e–03	–	9.8e–03	–	4.3e–04	–	2.2e–03	–
	2	1.3e–04	3.02	5.7e–04	3.09	1.4e–03	2.81	3.2e–05	3.75	1.4e–04	3.95
	3	1.6e–05	3.01	6.9e–05	3.05	1.9e–04	2.92	2.1e–06	3.90	9.3e–06	3.97
	4	2.0e–06	3.01	8.5e–06	3.01	2.4e–05	2.96	1.4e–07	3.95	5.8e–07	4.00
	5	2.5e–07	3.00	1.1e–06	2.99	3.0e–06	2.98	8.8e–09	3.98	3.8e–08	3.93
3	1	1.1e–04	–	4.8e–04	–	1.1e–03	–	3.8e–05	–	1.8e–04	–
	2	6.8e–06	4.00	2.9e–05	4.05	8.0e–05	3.85	1.3e–06	4.85	5.4e–06	5.09
	3	4.2e–07	4.00	1.8e–06	4.00	5.2e–06	3.93	4.3e–08	4.93	1.8e–07	4.89
	4	2.6e–08	4.00	1.1e–07	3.99	3.4e–07	3.97	1.4e–09	4.97	6.0e–09	4.93
	5	1.7e–09	4.00	7.1e–09	4.00	2.1e–08	3.98	4.3e–11	4.98	1.9e–10	5.00
4	1	8.0e–06	–	3.5e–05	–	8.7e–05	–	1.9e–06	–	8.9e–06	–
	2	2.5e–07	4.98	1.1e–06	5.02	3.0e–06	4.87	3.3e–08	5.82	1.4e–07	5.99
	3	7.9e–09	4.99	3.4e–08	4.99	9.7e–08	4.94	5.4e–10	5.94	2.4e–09	5.89
	4	2.5e–10	5.00	1.1e–09	5.00	3.1e–09	4.98	8.7e–12	5.97	3.7e–11	6.01
	5	7.8e–12	5.00	3.4e–11	4.98	9.7e–11	4.99	6.5e–13	3.74	6.4e–12	2.52

Example 4.3. Consider the following one dimensional traveling wave, solution of (1) with periodic boundary conditions

$$u(t, x) = \sin(2n\pi(x - t)), \quad x \in (0, 1), t \in (0, T_f], \tag{32}$$

with parameter $\kappa = 1$. Firstly, we test the dissipation properties of the HDG schemes with low frequency, $n = 1$. For a fixed triangulation, we compute the numerical approximations by the dissipative scheme [26] until its amplitude decays to a 80% of the amplitude of the exact solution, registering the time at which this occurs. Next, for the same final time and triangulation we compute the numerical approximations by the implicit symplectic scheme HDG-SDIRK. We display the graph of the exact solutions and numerical approximations in Fig. 1. We observe that whilst the approximations by the dissipative scheme decay in amplitude, the approximations by the symplectic scheme maintains it.
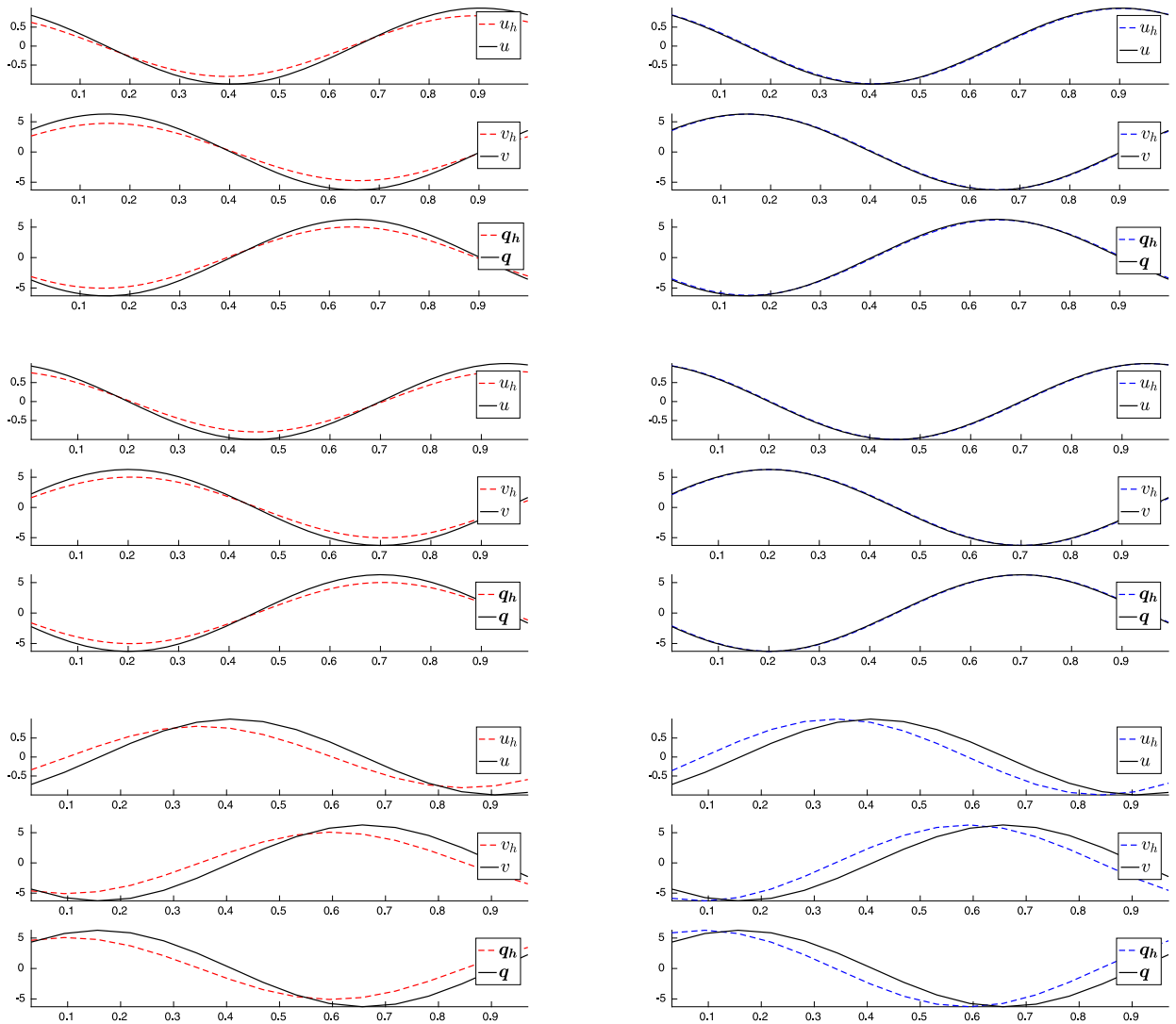
Fig. 1. Example 4.3. Plot of exact solution and numerical approximations by the dissipative implicit scheme (left) and Hamiltonian implicit scheme (right). We use a symplectic time integrator DIRK of order 6 with time step $\Delta t = h$ for both cases. Top row: mesh size $h = 2^{-8}$, polynomial degree $k = 0$, and final time $T_f = 0.65$. Middle row: mesh size $h = 2^{-6}$, polynomial degree $k = 1$, and final time $T_f = 551.70$. Bottom row: mesh size $h = 2^{-4}$, polynomial degree $k = 2$, and final time $T_f = 5944.16$.

Secondly, we consider the exact solution (32) with a higher frequency, $n = 6$. For a given mesh parameter, we compute the dissipative and symplectic implicit approximations until a given (reasonably small) final time $T_f = 20$. Fig. 2 shows the exact solution and approximations at the final time. We observe the same behavior than in the low frequency case, this time magnified by the higher frequency. In addition, we compute the energy associated to the schemes, and display in Fig. 3 their relative errors in time. To study the effect on the energy of the terms over the skeleton of the triangulation, we compute the following modified energy for the symplectic scheme

$$\widetilde{H}_h(u_h, v_h) = \frac{1}{2}(v_h, v_h)_{\Omega_h} + \frac{1}{2}(\kappa^{-1}\boldsymbol{q}_h, \boldsymbol{q}_h)_{\Omega_h}. \tag{33}$$

As seen Fig. 3, although $\widetilde{H}_h$ has similar error as H_h, it is not constant in time. The plots of the numerical approximations and the energies show the outstanding dissipative properties of our scheme in comparison with the dissipative scheme.

Example 4.4. Consider an initial pulse of the form

$$\phi_{b,\delta}(x) = \psi\left(\frac{x-b}{\delta}\right), \qquad \psi(x) = \begin{cases} (2x-1)^{10}(2x+1)^{10}, & \text{if } |x| < 0.5 \\ 0, & \text{otherwise.} \end{cases} \tag{34}$$
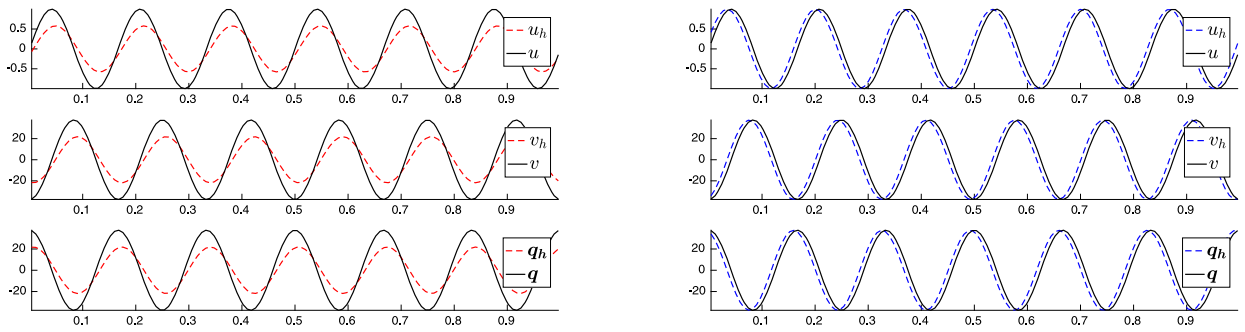
Fig. 2. Example 4.3. Plot of exact solution ($n = 6$) and numerical approximations by the dissipative implicit scheme (left) and symplectic implicit scheme (right). We use a symplectic time integrator of order 6 with time step $\Delta t = h$ for both cases.
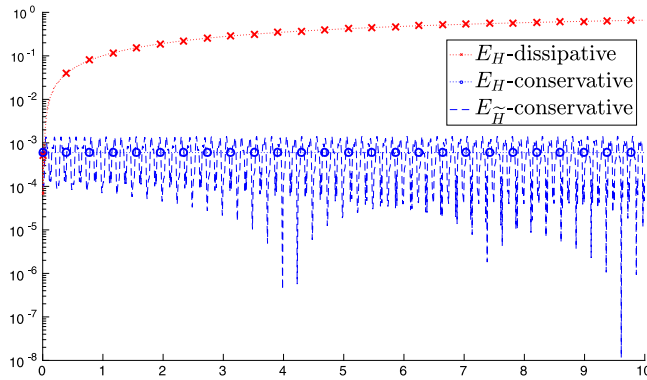
Fig. 3. Example 4.3. Semi-log plot of the relative errors of the discrete energies vs. time. We plot the relative error of the discrete energy, $E_H = |H - H_h|/H$, where H is the exact energy and where the discrete energies H_h, defined in (13), are provided by the dissipative and conservative schemes. We also plot the relative error of the energy $\widetilde{H}_h$, defined in (33), $E_{\widetilde{H}} = |H - \widetilde{H}_h|/H$, computed by the conservative scheme. We use a symplectic time integrator of order 6 with time step $\Delta t = h = 2^{-6}$, and $\tau = 10$.
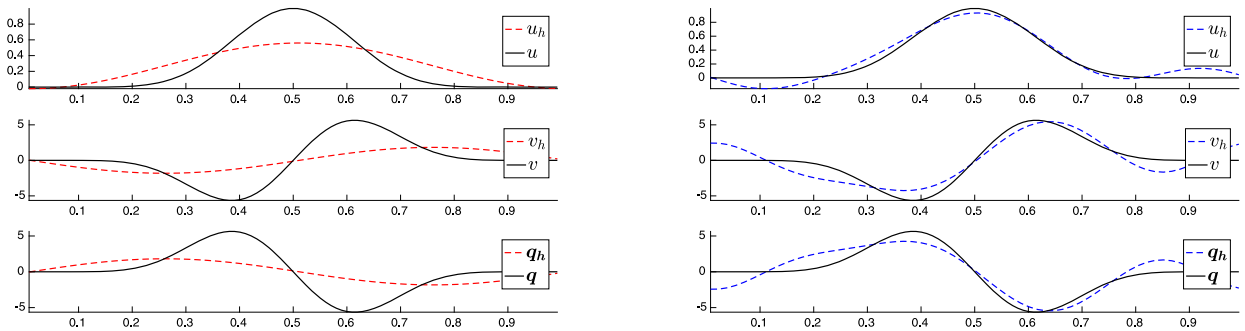
Fig. 4. Example 4.4. Plot of the exact solution and numerical approximations by the implicit dissipative (left) and Hamiltonian schemes (right) for $k = 1$. We use a triangulation with mesh size $h = 2^{-6}$, and a time integrator DIRK of order 6 with time step $\Delta t = h$, up to the final time $T_f = 1000$.

We consider the following exact solution of the wave equation (1) with periodic boundary conditions:

$$u(t, x) = \phi_{b,\delta}(x - t),$$

with $b = 1/2$, and $\delta = 1$ in (34). We test the long time behavior of the numerical approximations. We compute the piecewise linear approximations by the dissipative scheme and HDG-SDIRK scheme using a DIRK formula of order 6, up to the final time $T_f = 1000$, for a fixed mesh parameter $h = 2^{-6}$ and time step $\Delta t = h$. We plot the approximate and exact solutions in Fig. 4. We observe that, in the long time term, the symplectic scheme has superior dissipation properties, and it captures the shape of the solution more accurately than the dissipative scheme. We plot the relative error of the discrete energies in Fig. 5. We observe that the energy for our scheme is constant in time, and the energy of dissipative scheme diminishes in time. Although $\widetilde{H}_h$ oscillates in time, its average is approximately constant.
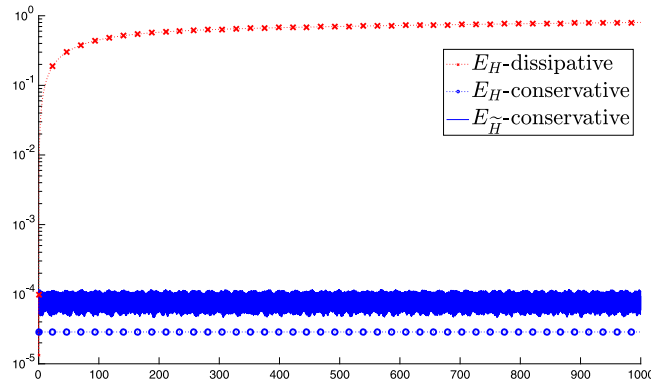
Fig. 5. Example 4.4. Semi-log plot of the relative errors of the discrete energies vs. time. We plot the relative error of the discrete energy, $E_H = |H - H_h|/H$, where H is the exact energy and where the discrete energies H_h, defined in (13), are provided by the dissipative and conservative schemes. We also plot the relative error of the energy $\widetilde{H}_h$, defined in (33), $E_{\widetilde{H}} = |H - \widetilde{H}_h|/H$, computed by the conservative scheme. We use a symplectic time integrator of order 6 with time step $\Delta t = h = 2^{-6}$, and $\tau = 10$.

Example 4.5. Consider the exact solution to the wave equation (1) in two dimensions with periodic boundary conditions,

$$u(t, x, y) = \phi_{b,\delta}(x - t), + \phi_{b,\delta}(y - t), \quad x, y \in (0, 1)^2,$$

with parameters $b = 1/2$, and $\delta = 1$ in the impulse function defined in (34). We proceed as in the previous example. We compute the piecewise linear approximations by the dissipative scheme and HDG-SDIRK scheme using a DIRK formula of order 5, up to the final time $T_f = 50$, for a fixed mesh parameter $h = 2^{-5}$ and time step $\Delta t = .25h$. We plot the approximate and exact solutions in Fig. 6. We observe that the symplectic scheme has superior dissipation properties in comparison with the dissipative scheme, even for this example where the final time is moderate. Thus, the approximation by the symplectic scheme becomes quickly more accurate.

Example 4.6. We consider exact solution $u(t, x) = \sin(2\pi(t + x))$, on a periodic domain $(0, 1)$, and compare the energies obtained by the HDG symplectic Euler and HDG implicit midpoint methods. We compute with polynomials of order $k = 0$ and $k = 1$ until the final time $T_f = 10$. We plot the relative energies in Fig. 7, observing oscillations in the case of the symplectic Euler whilst the energy in the case of the implicit midpoint remains constant. The exact conservation of the Hamiltonian is due to the fact that the implicit midpoint scheme preserves quadratic invariants, which is the case of our discrete Hamiltonian. We observe that the other Runge–Kutta methods (implicit and partitioned explicit) used in this paper show the same invariant behavior. Similar results are also obtained with higher-order polynomials.

5. Extensions and concluding remarks

In this Section, we extend our semi-discrete scheme to other finite element methods, in particular Discontinuous Galerkin methods. We prove that the resulting scheme also preserves the Hamiltonian structure of the wave equation, and hence, it is energy-conservative. We then mention possible applications of our ideas to other Hamiltonian equations.

5.1. Hamiltonian Discontinuous Galerkin methods

For the sake of simplicity, we consider in this section the wave equation with periodic boundary conditions. We first introduce standard Discontinuous Galerkin (DG) notation for the averages and jumps on faces of the triangulation
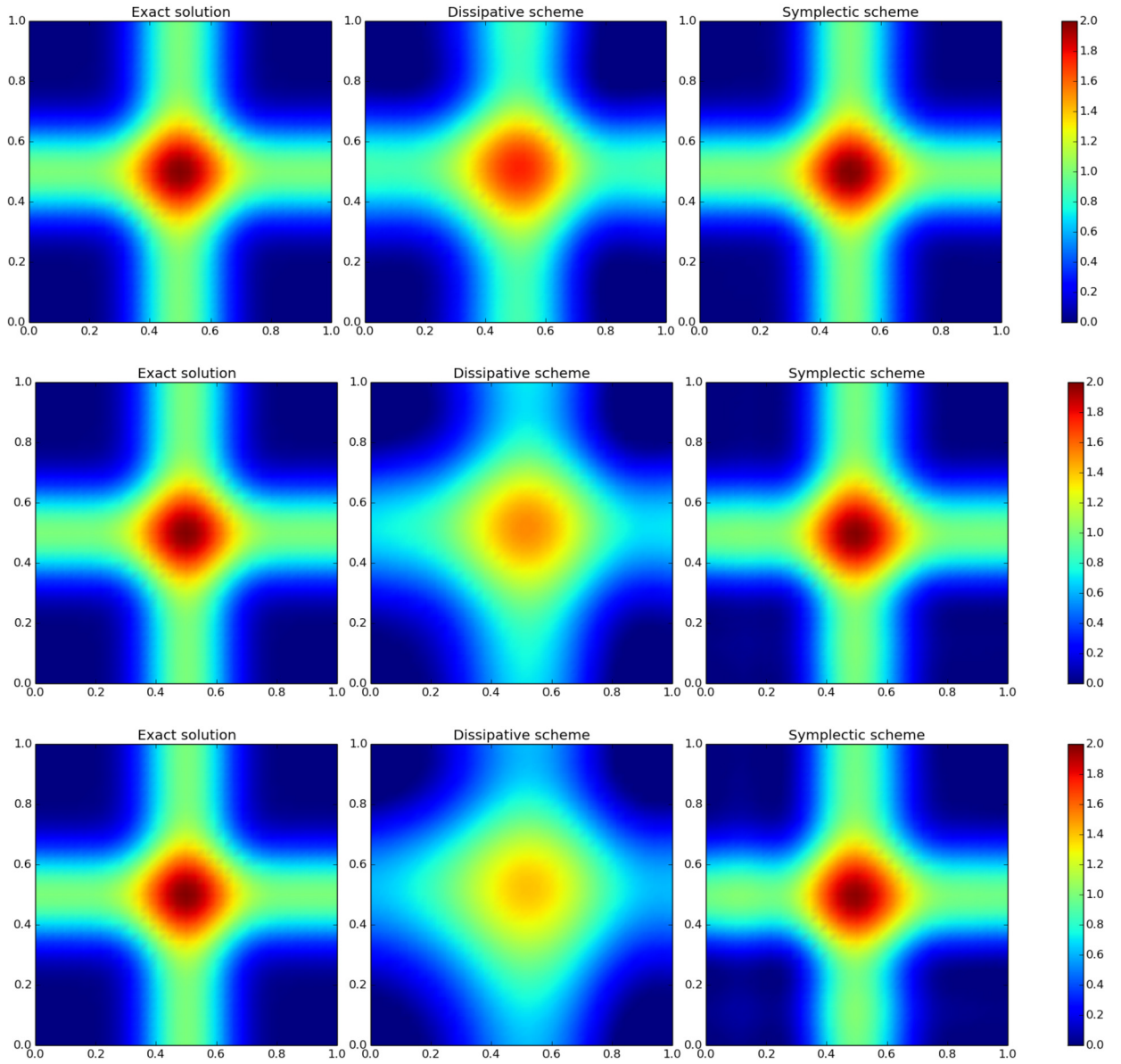
$$\{u\} := \frac{1}{2}(u^+ + u^-), \qquad \{q\} := \frac{1}{2}(q^+ + q^-),$$
$$[\![u]\!] := u^+ n^+ + u^- n^-, \quad [\![q]\!] := q^+ \cdot n^+ + q^- \cdot n^-.$$

We also introduce the dot product over the set of faces of the triangulation

$$\langle \cdot, \cdot \rangle_{\mathcal{E}_h} := \sum_{F \in \mathcal{E}_h} \langle \cdot, \cdot \rangle_F. \tag{35}$$

By means of the previous definitions for averages and jumps we have the following relation

$$\langle \mu, \eta \rangle_{\partial \Omega_h} = \langle \{\mu\} [\![\eta]\!] + \{\eta\} [\![\mu]\!], 1 \rangle_{\mathcal{E}_h}, \tag{36}$$

Fig. 6. Example 4.4. Contour plots at $T_f = 10$ (first row), $T_f = 30$ (second row), and $T_f = 50$ (third row): exact solution (left), numerical approximation by the dissipative scheme in [26] (center), and numerical approximation by the HDG-symplectic (right). Parameters: $k = 1$, $h = 2^{-5}$, and $\Delta t = h/4$. Time integrator symplectic DIRK(6, 5).

for $\mu, \eta \in L^2(\mathcal{E}_h)$. Now, we introduce the semi-discrete DG scheme: find $(u_h(t), v_h(t), \boldsymbol{q}_h(t)) \in W_h \times W_h \times \boldsymbol{V}_h$, such that

$$(\dot{u}_h(t), w)_{\Omega_h} = (v(t), w)_{\Omega_h} \tag{37a}$$

$$(\dot{v}_h(t), w)_{\Omega_h} = (\boldsymbol{q}_h(t), \nabla w)_{\Omega_h} - \langle \widehat{\boldsymbol{q}}_h(t) \cdot \boldsymbol{n}, w \rangle_{\partial \Omega_h} + (f(t), w)_{\Omega_h} \tag{37b}$$

$$(\kappa^{-1} \boldsymbol{q}_h(t), \boldsymbol{r})_{\Omega_h} = (u_h(t), \nabla \cdot \boldsymbol{r})_{\Omega_h} - \langle \widehat{u}_h(t), \boldsymbol{r} \cdot \boldsymbol{n} \rangle_{\partial \Omega_h} \tag{37c}$$

where the numerical fluxes are explicitly defined on the faces $F \in \mathcal{F}_h \backslash \partial \Omega$ by:

$$\widehat{\boldsymbol{q}}_h := \{\!\!\{\boldsymbol{q}_h\}\!\!\} + C_{11}[\![u_h]\!] - \boldsymbol{C}_{12}[\![\boldsymbol{q}_h]\!], \qquad \widehat{u}_h := \{\!\!\{u_h\}\!\!\} + \boldsymbol{C}_{12} \cdot [\![u_h]\!] + C_{22}[\![\boldsymbol{q}_h]\!],$$

with auxiliary parameters C_{11}, $\boldsymbol{C}_{12}$ and C_{22}, that might depend on x. These parameters define different DG methods. For example, for $C_{22} \equiv 0$ we obtain the LDG method.
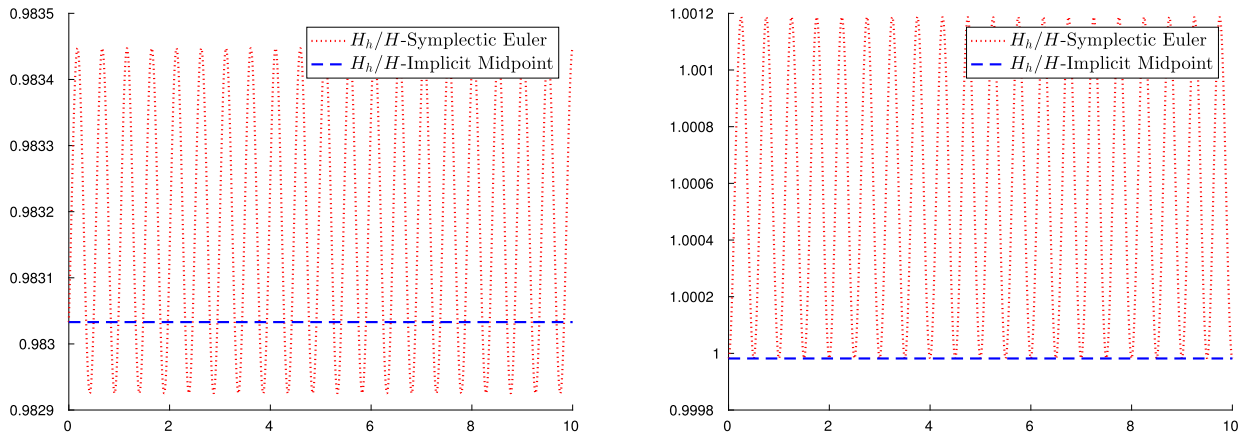
Fig. 7. Relative energies vs. time. We plot the relative energies H_h/H, where H is the exact energy and H_h, defined in (13), are computed by the conservative HDG scheme with two time integrators, the symplectic Euler and the implicit midpoint method. Left figure: polynomial degree $k = 0$, $\Delta t = h = 2^{-8}$ and $\tau = 10$. Right figure: polynomial degree $k = 1$, $\Delta t = .5h = 2^{-7}$ and $\tau = 10$.

The discrete (total) Hamiltonian function is defined by:

$$H_h(u_h, v_h, t) = \frac{1}{2}(v_h, v_h)_{\Omega_h} + \frac{1}{2}(\kappa^{-1}\boldsymbol{q}_h, \boldsymbol{q}_h)_{\Omega_h} + \frac{1}{2}C_{11}\langle[\![u_h]\!], [\![u_h]\!]\rangle_{\mathcal{E}_h} + \frac{1}{2}C_{22}\langle[\![\boldsymbol{q}_h]\!], [\![\boldsymbol{q}_h]\!]\rangle_{\mathcal{E}_h} - (f(t), u_h)_{\Omega_h}. \quad (38)$$

Thus, we prove that formulation (37) has a Hamiltonian structure.

Theorem 3. *Set* $\mathsf{p}_i := v_i$ *and* $\mathsf{q}_i := u_i$, *for* $i \in \mathcal{J}$, *and* $\mathcal{H}(\mathsf{p}, \mathsf{q}, t) := H_h(u_h, v_h, t)$. *Then, the DG method* (37) *is equivalent to the following Hamiltonian system:*

$$\dot{\mathsf{p}}_i = -\frac{\partial}{\partial \mathsf{q}_i}\mathcal{H}(\mathsf{p}, \mathsf{q}, t) \quad i \in \mathcal{J}, \quad (39a)$$

$$\dot{\mathsf{q}}_i = \frac{\partial}{\partial \mathsf{p}_i}\mathcal{H}(\mathsf{p}, \mathsf{q}, t) \quad i \in \mathcal{J}. \quad (39b)$$

For the sake of completeness, we provide the proof in the Appendix.

Theorem 3 implies that if we pair the DG semi-discrete scheme (37) with a symplectic time integrator we obtain a fully discrete energy conservative DG method. These methods certainly have attractive properties. For instance, the locality of the LDG method together with explicit time integrators (for example, ESPRK) gives fast fully discrete scheme with conservation properties. On the other hand, the superconvergence properties of the HDG have the edge in terms of accuracy.

5.2. Concluding remarks

In this paper, we devised Hamiltonian HDG methods for approximating solutions of the wave equation. The semi-discrete HDG methods are said to be Hamiltonian since they satisfy a finite dimensional Hamiltonian system, for a discrete Hamiltonian functional approximating the infinite dimensional Hamiltonian functional of the equation. Then, the Hamiltonian structure of the method implies that the discrete energy is conserved in time. As is shown in [14], the L^2 errors of the semi-discrete method converge optimally with an order of $k + 1$, when piecewise polynomial spaces of degree k are used. The method also has superconvergence properties that allow constructing a post-processed displacement approximation, which converges with order $k + 2$. Similarly, we presented a post-processed approximation for the velocity which super converges with order $k + 2$.

We take advantage of the Hamiltonian structure of the semi-discrete HDG scheme using symplectic time integrators for the discretization in time. In particular, we considered symplectic diagonally implicit Runge–Kutta methods and explicit symplectic partitioned Runge–Kutta methods. These time-stepping schemes were chosen, in order to match the high-order accuracy properties of our spatial discretizations, and hence, achieving high-order accurate approximations, and because they are known to preserve quadratic invariants. We corroborated the optimal convergence and superconvergence properties of the fully discrete schemes with numerical examples, and compared our energy-conservative schemes with the dissipative scheme introduced in [26], evidencing the superior conservative and dissipative properties of our fully discrete schemes.

We concluded our analysis observing that the keystone of our numerical methods, the Hamiltonian structure, is not an exclusive feature of the HDG discretization. We commented that discontinuous Galerkin and Mixed methods also have this property. In particular, we presented a proof of the Hamiltonian structure of a general discretization using discontinuous Galerkin methods.

Table A.1
Coefficients of schemes of the SDRIK(q, p) schemes. From left to right: SDIRK(3, 3), SDIRK(3, 4), SDIRK(6, 5), and SDIRK(7, 6). For the first two schemes $a = 1.351207191959658$.

i	b_i		i	b_i		i	b_i		i	b_i
1	a		1	a		1	0.5080048194000274		1	7.8451361047755652e-01
2	a		2	$1 - 2a$		2	1.360107162294827		2	2.3557321335935860e-01
3	$1 - 2a$		3	a		3	2.0192933591817224		3	−1.1776799841788705
						4	0.5685658926458251		4	1.3151863206839107
						5	−1.4598520495864393		5	−1.1776799841788705
						6	−1.9961191839359627		6	2.3557321335935860e-01
									7	7.8451361047755652e-01

Table A.2
Coefficients of the schemes ESPRK(q, p) schemes. Top, from the left to right: ESPRK(3, 3) (Ruth's method) [29], ESPRK(6, 4) [22], and ESPRK(6, 5) [24]. Bottom: ESPRK(11, 6) [1].

i	b_i	$\tilde{b}_i$		i	b_i	$\tilde{b}_i$		i	b_i	$\tilde{b}_i$
1	7/24	2/3		1	7/48	1/3		1	0.1193900292875672758	0.3398839625839110000
2	3/4	−2/3		2	3/8	−1/3		2	0.6989273703824752308	−0.088601336903027329
3	−1/24	1		3	−1/48	1		3	−0.1713123582716007754	0.5858564768259621188
				4	−1/48	−1/3		4	0.4012695022513534480	−0.6030393565364911888
				5	3/8	1/3		5	0.0107050818482359840	0.3235807965546976394
				6	7/48	0		6	−0.0589796254980311632	0.4423637942197494587

i	b_i	$\tilde{b}_i$
1	0.0502627644003922	0.148816447901042
2	0.413514300428344	−0.132385865767784
3	0.0450798897943977	0.067307604692185
4	−0.188054853819569	0.432666402578175
5	0.541960678450780	−0.016404589403618
6	−0.725525558508690	−0.016404589403618
7	0.541960678450780	0.432666402578175
8	−0.188054853819569	0.067307604692185
9	0.0450798897943977	−0.132385865767784
10	0.413514300428344	0.148816447901042
11	0.0502627644003922	0

Finally, regarding our future research directions, we reiterate that the fundamental idea behind our energy-conservative methods is the discrete preservation of the Hamiltonian structure of the problem. Although we have only dealt with a linear wave equation, all we have done here carries over to non-linear systems of equations with a Hamiltonian structure. We plan to extend our approach to other linear and nonlinear Hamiltonian systems including the elastodynamics (small and large deformation) equations, Maxwell equations, and shallow water equations.

Acknowledgements

Appendix A. Runge–Kutta coefficients

A.1. Symplectic DIRK schemes

In Table A.1, we display the coefficients of the Symplectic Diagonally Implicit Runge–Kutta schemes, of q-stages and p-order, SDIRK(q, p), that are used in our computations.

A.2. Symplectic EPRK schemes

In Table A.2, we display the coefficients of the Explicit Symplectic Partitioned Runge–Kutta schemes, of q-stages and p-order, ESPRK(q, p), that are used in our computations.

Appendix B. Proof of Theorem 3

Let us prove the first identity. We have

$$\dot{\mathsf{p}}_i = \dot{v}_i \qquad\qquad \text{by def. of } \mathsf{p}_i,$$

$$= (\dot{v}_h, \phi_i)_{\Omega_h} \qquad\qquad \text{by def. of } \phi_i,$$

$$= (\nabla\phi_i, \boldsymbol{q}_h)_{\Omega_h} - \langle\phi_i, \widehat{\boldsymbol{q}}_h \cdot \boldsymbol{n}\rangle_{\partial\Omega_h} + (\phi_i, f(t))_{\Omega_h} \qquad\qquad \text{by (37)},$$

$$= -(\phi_i, \nabla\cdot\boldsymbol{q}_h)_{\Omega_h} - \langle\phi_i, (\widehat{\boldsymbol{q}}_h - \boldsymbol{q}_h)\cdot\boldsymbol{n}\rangle_{\partial\Omega_h} + (\phi_i, f(t))_{\Omega_h}$$

$$= -(\frac{\partial}{\partial u_i}u_h, \nabla\cdot\boldsymbol{q}_h)_{\Omega_h} - \langle\frac{\partial}{\partial u_i}u_h, (\widehat{\boldsymbol{q}}_h - \boldsymbol{q}_h)\cdot\boldsymbol{n}\rangle_{\partial\Omega_h} + (\frac{\partial}{\partial u_i}u_h, f(t))_{\Omega_h} \qquad \text{by def. of } \phi_i,$$

$$= -(\frac{\partial}{\partial u_i}u_h, \nabla\cdot\boldsymbol{q}_h)_{\Omega_h} + \langle\frac{\partial}{\partial u_i}\widehat{u}_h, \boldsymbol{q}_h\cdot\boldsymbol{n}\rangle_{\partial\Omega_h} - \langle\frac{\partial}{\partial u_i}(u_h - \widehat{u}_h), (\widehat{\boldsymbol{q}}_h - \boldsymbol{q}_h)\cdot\boldsymbol{n}\rangle_{\partial\Omega_h}$$

$$\quad + (\frac{\partial}{\partial u_i}u_h, f(t))_{\Omega_h}$$

$$= -(\frac{\partial}{\partial u_i}u_h, \nabla\cdot\boldsymbol{q}_h)_{\Omega_h} + \langle\frac{\partial}{\partial u_i}\widehat{u}_h, \boldsymbol{q}_h\cdot\boldsymbol{n}\rangle_{\partial\Omega_h} + (\frac{\partial}{\partial u_i}u_h, f(t))_{\Omega_h}$$

$$\quad - \langle\frac{\partial}{\partial u_i}(\{u_h - \widehat{u}_h\})[\![\widehat{\boldsymbol{q}}_h - \boldsymbol{q}_h]\!] + \frac{\partial}{\partial u_i}([\![u_h - \widehat{u}_h]\!])\{\widehat{\boldsymbol{q}}_h - \boldsymbol{q}_h\}, 1\rangle_{\mathcal{E}_h}$$

$$= -(\frac{\partial}{\partial u_i}\boldsymbol{q}_h, \boldsymbol{q}_h)_{\Omega_h} + (\frac{\partial}{\partial u_i}u_h, f(t))_{\Omega_h}$$

$$\quad - \langle-\frac{\partial}{\partial u_i}(\{u_h - \widehat{u}_h\})[\![\boldsymbol{q}_h]\!] + \frac{\partial}{\partial u_i}([\![u_h]\!])\{\widehat{\boldsymbol{q}}_h - \boldsymbol{q}_h\}, 1\rangle_{\mathcal{E}_h}$$

$$= -(\frac{\partial}{\partial u_i}\boldsymbol{q}_h, \boldsymbol{q}_h)_{\Omega_h} + (\frac{\partial}{\partial u_i}u_h, f(t))_{\Omega_h}$$

$$\quad - \langle\frac{\partial}{\partial u_i}(\boldsymbol{C}_{12}[\![u_h]\!] + C_{22}[\![\boldsymbol{q}_h]\!])[\![\boldsymbol{q}_h]\!] + \frac{\partial}{\partial u_i}([\![u_h]\!])(C_{11}[\![u_h]\!] - \boldsymbol{C}_{12}[\![\boldsymbol{q}_h]\!]), 1\rangle_{\mathcal{E}_h}$$

$$= -(\frac{\partial}{\partial u_i}\boldsymbol{q}_h, \boldsymbol{q}_h)_{\Omega_h} + (\frac{\partial}{\partial u_i}u_h, f(t))_{\Omega_h}$$

$$\quad - C_{22}\frac{\partial}{\partial u_i}\langle[\![\boldsymbol{q}_h]\!][\![\boldsymbol{q}_h]\!], 1\rangle_{\mathcal{E}_h} - C_{11}\frac{\partial}{\partial u_i}\langle[\![u_h]\!][\![u_h]\!], 1\rangle_{\mathcal{E}_h}$$

$$= -\frac{\partial}{\partial u_i}H_h(u_h, v_h, t) \qquad\qquad \text{by (38)},$$

$$= -\frac{\partial}{\partial \mathsf{q}_i}\mathcal{H}(\mathsf{p}, \mathsf{q}, t),$$

by definition of $\mathcal{H}(\mathsf{p}, \mathsf{q}, t)$.

The proof of the second identity follows in a similar manner. This completes the proof. $\square$

References

[1] S. Blanes, P.C. Moan, Practical symplectic partitioned Runge–Kutta and Runge–Kutta–Nyström methods, J. Comput. Appl. Math. 142 (2) (2002) 313–330.

[2] P.B. Bochev, C. Scovel, On quadratic invariants and symplectic structure, BIT 34 (3) (1994) 337–345.

[3] P. Brenner, L.R. Scott, The Mathematical Theory of Finite Element Methods, Texts in Applied Mathematics, vol. 15, Springer Verlag, 1994.

[4] E.T. Chung, B. Engquist, Optimal discontinuous Galerkin methods for the acoustic wave equation in higher dimensions, SIAM J. Numer. Anal. 47 (5) (2009) 3820–3848.

[5] E.T. Chung, B. Engquist, Optimal discontinuous Galerkin methods for the acoustic wave equation in higher dimensions, SIAM J. Numer. Anal. 47 (5) (2009) 3820–3848.

[6] P. Ciarlet, The Finite Element Method for Elliptic Problems, North-Holland, Amsterdam, 1978.

[7] B. Cockburn, Discontinuous Galerkin methods for computational fluid dynamics, in: E. Stein, R. de Borst, T.J.R. Hughes (Eds.), Encyclopedia of Computational Mechanics, second edition, vol. 3, John Wiley & Sons, Ltd., England, 2016, in press, 111 pages.

[8] B. Cockburn, Static condensation, hybridization, and the devising of the HDG methods, in: G.R. Barrenechea, F. Brezzi, A. Cagniani, E.H. Georgoulis (Eds.), Building Bridges: Connections and Challenges in Modern Approaches to Numerical Partial Differential Equations, in: Lect. Notes Comput. Sci. Engrg., vol. 114, Springer Verlag, Berlin, 2016, pp. 129–177, LMS Durham Symposia funded by the London Mathematical Society, Durham, U.K., on July 8–16, 2014.

[9] B. Cockburn, G. Fu, Superconvergence by M-decompositions. Part II: construction of two-dimensional finite elements, Modél. Math. Anal. Numér. 51 (1) (2017) 165–186.

[10] B. Cockburn, G. Fu, Superconvergence by M-decompositions. Part III: construction of three-dimensional finite elements, Modél. Math. Anal. Numér. 51 (1) (2017) 365–398.

[11] B. Cockburn, G. Fu, F.-J. Sayas, Superconvergence by M-decompositions. Part I: general theory for HDG methods for diffusion, Math. Comput. 86 (306) (2017) 1609–1641.

[12] B. Cockburn, J. Gopalakrishnan, R. Lazarov, Unified hybridization of discontinuous Galerkin, mixed and continuous Galerkin methods for second order elliptic problems, SIAM J. Numer. Anal. 47 (2009) 1319–1365.

[13] B. Cockburn, V. Quenneville-Bélair, Uniform-in-time superconvergence of HDG methods for the acoustic wave equation, Math. Comput. 83 (2014) 65–85.
[14] Bernardo Cockburn, Zhixing Fu, Allan Hungria, Liangyue Ji, Manuel A. Sánchez, Francisco-Javier Sayas, Stormer–Numerov HDG methods for acoustic waves, J. Sci. Comput. (Sep. 2017), http://dx.doi.org/10.1007/s10915-017-0547-z.
[15] G.J. Cooper, Stability of Runge–Kutta methods for trajectory problems, IMA J. Numer. Anal. 7 (1) (1987) 1–13.
[16] L.C. Cowsar, T.F. Dupont, M.F. Wheeler, A priori estimates for mixed finite element methods for the wave equation, in: Reliability in Computational Mechanics, Austin, TX, 1989, Comput. Methods Appl. Mech. Eng. 82 (1–3) (1990) 205–222.
[17] L. Beirão da Veiga, L. Lopez, G. Vacca, Mimetic finite difference methods for Hamiltonian wave equations in 2d, Comput. Math. Appl. 74 (5) (2017) 1123–1141, SI: SDS2016—Methods for PDEs.
[18] R.S. Falk, G.R. Richter, Explicit finite element methods for symmetric hyperbolic equations, SIAM J. Numer. Anal. 36 (1999) 935–952.
[19] T. Geveci, On the application of mixed finite element methods to the wave equations, RAIRO Modél. Math. Anal. Numér. 22 (2) (1988) 243–250.
[20] M.J. Gröte, A. Schneebeli, D. Schötzau, Discontinuous Galerkin finite element method for the wave equation, SIAM J. Numer. Anal. 44 (6) (2006) 2408–2431.
[21] E. Hairer, C. Lubich, G. Wanner, Geometric Numerical Integration: Structure-Preserving Algorithms for Ordinary Differential Equations, Springer Series in Computational Mathematics, Springer, Berlin, Heidelberg, New York, 2006.
[22] E. Hairer, S.P. Nørsett, G. Wanner, Solving Ordinary Differential Equations I: Nonstiff Problems, 2nd revised ed., Springer-Verlag New York, Inc., New York, NY, USA, 1993.
[23] R.C. Kirby, T.T. Kieu, Symplectic-mixed finite element approximation of linear acoustic wave equations, Numer. Math. 130 (2) (2015) 257–291.
[24] R.I. McLachlan, P. Atela, The accuracy of symplectic integrators, Nonlinearity 5 (2) (1992) 541–562.
[25] P. Monk, G.R. Richter, A discontinuous Galerkin method for linear symmetric hyperbolic systems in inhomogeneous media, J. Sci. Comput. 22 and 23 (2003) 443–477.
[26] N.C. Nguyen, J. Peraire, Hybridizable discontinuous Galerkin methods for partial differential equations in continuum mechanics, J. Comput. Phys. 231 (2012) 5955–5988.
[27] S. Petersen, C. Farhat, R. Tezaur, A space–time discontinuous Galerkin method for the solution of the wave equation in the time domain, Int. J. Numer. Methods Eng. 78 (2009) 275–295.
[28] S. Piperno, Symplectic local time-stepping in non-dissipative DGTD methods applied to wave propagation problems, M2AN Math. Model. Numer. Anal. 40 (5) (2006) 815–841.
[29] R.D. Ruth, A canonical integration technique, IEEE Trans. Nucl. Sci. (1983) 2669–2671.
[30] J.M. Sanz-Serna, Symplectic integrators for Hamiltonian problems: an overview, in: Acta Numerica, 1992, in: Acta Numer., Cambridge Univ. Press, Cambridge, 1992, pp. 243–286.
[31] M. Stanglmeier, N.C. Nguyen, J. Peraire, B. Cockburn, An explicit hybridizable discontinuous Galerkin method for the acoustic wave equation, Comput. Methods Appl. Mech. Eng. 300 (2016) 748–769.
[32] Y. Xing, C.-S. Chou, C.-W. Shu, Energy conserving local discontinuous Galerkin methods for wave propagation problems, Inverse Probl. Imaging 7 (3) (2013) 967–986.